

Customer No.: 31561  
Application No.: 10/710,488  
Docket No.: 10304-US-PA

### **REMARKS**

#### **Present Status of the Application**

Claim 1 is objected to because "to exposed" should have been "to expose". The Office Action rejected claims 1-22 under 35 U.S.C. 112, first paragraph, as failing to comply with the enablement requirement. The Office Action also rejected claims 1, 10 and 19 under 35 U.S.C. 112, second paragraph, because there is insufficient antecedent basis in the claims.

Applicants have amended claims 1, 10 and 19 to more clearly define the present invention. After entry of the foregoing amendments, claims 1-22 remain pending in the present application, and reconsideration of those claims is respectfully requested.

#### **Claim Objections**

Claim 1 is objected to because "to exposed" should have been "to expose". Applicant has amended "to exposed" into "to expose" in claim 1 to overcome the objection.

#### **Rejection under 35 U.S.C 112, first paragraph**

The office action points out claims 1-22 contains subject matter, which was not described in the specification in such a way as to enable one skilled in the art to which it pertains, or with which it is most nearly connected, to make and/or use the invention. Specification only discloses etching the (hard) mask layer using a patterned photoresist layer but does not provide any clear

Customer No.: 31561  
Application No.: 10/710,488  
Docket No.: 10304-US-PA

explanation how to form the plurality of micro-trenches that one of skilled in the art reasonable practices the invention.

Applicant respectfully traverses the rejections for at least the reasons set forth below. In the specification of the present application, in Fig. 1B, using the patterned photoresist layer 108 as etching mask, the hard mask layer 104 is etched. Due to the trenching effect, a portion of the hard mask layer 104 remained in the exposed region 120, and micro-trenches 110 are formed at the edges of the exposed region 120 (see paragraph [0020] of the specification). In other words, the micro-trenches 110 can be formed due to the trenching effect in an etching process. As a matter of fact, the trenching effect is happened or existed in an etching process that is well known to the people skilled in the art. Conventionally, the trenching effect is undesired when an etching process is performed to pattern a film layer (see paragraph [0019] of the specification). However, the present invention utilizes the trenching effect in an etching process to form micro-trenches.

Applicant also provides four references to show the trenching effect is prior art and is well known to the people skilled in the art. In particular, the reference of "Robert J. H., Mark J. K., Microtrenching resulting from specular reflection during chlorine etching of silicon, *J. Vac. Sci Technol.* B 16(4), July/Aug 1998, pp 2102-2104" describes that *microtrenching refers to profiles for which the etch rate is larger near the corners of a trench compared to the center of the trench*. The etch profile across the floor of the trench is therefore either convex or has vertical slots at the base of the sidewalls (see lines 9-13, first paragraph, page 2102). This

Customer No.: 31561  
Application No.: 10/710,488  
Docket No.: 10304-US-PA

reference also describes that microtrenches was first discussed by Nguyen et al. (*Electrochem. Soc.* 138, 1112 (1991) (lines 23-24, first paragraph, page 2102).

Because the micro-trenches are formed due to the trenching effect in an etching process which has been described in the specification and the trenching effect is well known to the people skilled in the art, applicant submits people skilled in the art can practice the invention according the written description of the specification.

**Rejection under 35 U.S.C 112, second paragraph**

The office action rejected claims 1 and 10 because the limitation "due to the trenching effect" lacks antecedent basis in the claims. The office action also rejected claim 19 since there is insufficient antecedent basis for the limitation "the exposed region" in the claim.

Applicant has canceled "due to the trenching effect" in claims 1 and 10 to overcome the rejection.

Applicant has also amended claim 19 as below to overcome the rejection.

19. A method of reducing pattern pitch on a substrate, comprising the steps of:  
forming a material layer over the substrate;  
forming a patterned mask layer on the material layer to expose a region;  
performing an etching process by using the patterned mask layer as etching mask for forming micro-trenches in the material layer, wherein a residual material layer remains in the exposed region and the micro-trenches are formed along sidewalls of the patterned mask layer;  
and  
removing the patterned mask layer.

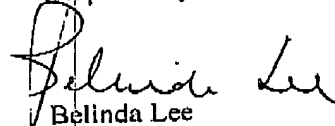
Customer No.: 31561  
Application No.: 10/710,488  
Docket No.: 10304-US-PA

**CONCLUSION**

For at least the foregoing reasons, it is believed that the pending claims are in proper condition for allowance. If the Examiner believes that a telephone conference would expedite the examination of the above-identified patent application, the Examiner is invited to call the undersigned.

Date: *March 7, 2006*

Respectfully submitted,

  
Belinda Lee

Registration No.: 46,863

Jianq Chyun Intellectual Property Office  
7<sup>th</sup> Floor-1, No. 100  
Roosevelt Road, Section 2  
Taipei, 100  
Taiwan  
Tel: 011-886-2-2369-2800  
Fax: 011-886-2-2369-7233  
Email: [belinda@jicpgroup.com.tw](mailto:belinda@jicpgroup.com.tw)  
[Usa@jicpgroup.com.tw](mailto:Usa@jicpgroup.com.tw)

## BEST AVAILABLE COPY

## Mask charging and profile evolution during chlorine plasma etching of silicon

K. H. A. Bogart,<sup>a)</sup> F. P. Klemens, M. V. Malyshev, J. I. Coloneil, V. M. Donnelly, and J. T. C. Lee  
Bell Laboratories, Lucent Technologies, Murray Hill, New Jersey 07974

J. M. Lane  
Department of Electrical Engineering, Massachusetts Institute of Technology, Cambridge, Massachusetts 02139

(Received 20 April 1999; accepted 6 August 1999)

Nonideal feature profile anomalies such as undercut, tapered, or bowed sidewalls and microtrenches at the base of trench sidewalls are often observed after etching masked silicon (Si) in chlorine ( $\text{Cl}_2$ ) plasmas. Off-normal impact with subsequent scattering and/or focusing of ions is believed to be the primary cause of these anomalies. Localized buildup of negative charge on the insulating mask sidewalls is one possible source of the ion deflection. Here we show that nearly identically shaped sidewalls and microtrenches were formed when Si features were etched in several  $\text{Cl}_2$  plasmas (the rf source and substrate bias powers and pressure were varied) regardless of whether the mask was insulating ( $\text{SiO}_2$ ) or conducting (Si or tungsten). Therefore, differential charging of the insulating mask material is not the fundamental cause of these profile characteristics. Ion angular distributions for each experimental plasma condition were estimated and the angle through which an ion would be deflected by a charged mask sidewall was calculated using simulated charged-mask field strengths reported in the literature. © 1999 American Vacuum Society. [S0734-211X(99)00406-0]

## I. INTRODUCTION

Sidewall profile control during etching in high-density, inductively coupled rf plasmas is essential for the production of gate electrodes and isolation trenches in  $<0.5 \mu\text{m}$  silicon-based transistor devices.<sup>1</sup> Transistor gates require vertical sidewalls, normal to the wafer surface, while tapered sidewalls are often beneficial for other applications including shallow trench isolation.<sup>2</sup> Unwanted profile anomalies such as microtrenches (Fig. 1) can form if the etching rate at the base of the trench sidewall is faster than the etching rate in the center of the trench.<sup>3-7</sup> Other undesirable deviations from straight sidewalls including undercut, tapered or bowed contours, and facet formation can occur during etching (Fig. 1).<sup>3,5,8-10</sup>

The mechanism by which these anomalous profiles form is believed to be a result of deviations in ion trajectories perpendicular to the wafer surface, prior to surface impact.<sup>3,5-8,11-13</sup> The ion angular distribution (IAD) determines the spatial variation of the ion flux on the feature surfaces during etching.<sup>14</sup> A broad IAD may increase ion impact and subsequent reflection from feature sidewalls, leading to the formation of microtrenches.<sup>3,5,7,12,14,15</sup> In high-pressure ( $>100 \text{ mTorr}$ ), relatively low-density ( $10^9$ – $10^{10} \text{ ions/cm}^3$ ) plasmas [reactive ion etching (RIE)], broadening of the IAD occurs through ion-neutral collisions and charge exchange reactions during transport across the plasma sheath.<sup>1,3,5,7,12</sup> In high-density ( $10^{11}$ – $10^{12} \text{ ions/cm}^3$ ), low-pressure ( $<50 \text{ mTorr}$ ) plasmas, however, the mean free path is  $>0.2 \text{ cm}$ , and increases in the IAD through collisions in the sheath are negligible.<sup>14,15</sup> The width of the IAD is deter-

mined from the ratio of the ion temperature ( $T_i$ ) in the plasma (near the sheath edge) to the sheath potential ( $E_{\text{sh}}$ ).<sup>14,15</sup> With typical IADs of  $1^\circ$ – $5^\circ$ ,<sup>14</sup> a substantial number of ions will impact feature sidewalls during etching. Ions (or hyperthermal neutrals) that impact the trench sidewalls at grazing angles ( $>80^\circ$ ) are largely specularly reflected and retain most of their energy.<sup>8,16,17</sup> Monte Carlo feature profile simulations by Hoekstra *et al.* for chlorine ( $\text{Cl}_2$ ) etching of silicon (Si) found that  $>90\%$  of ions reflected from trench sidewalls must be specular to reproduce the microtrenches observed experimentally.<sup>8</sup> If the sidewall contour is angled, the sidewall can act as a "lens" to focus the reflected ions to a small area at the base of the sidewall, enhancing the formation of microtrenches.<sup>8</sup> Mahorowala *et al.* have modeled  $\text{Cl}_2$  etching of  $\text{SiO}_2$ -masked polysilicon (poly-Si) with and without specular ion scattering, using IADs of  $2^\circ$ ,  $10^\circ$ , and  $20^\circ$ . Without ion scattering, the trench bottoms were rounded and the sidewalls were slightly bowed. The inclusion of ion scattering produced sharp microtrenches and the degree of the sidewall bow increased with broader IADs.<sup>11</sup>

Differential charging of mask materials has also been implicated as a significant contribution to alterations in the directionality of ions within an etching feature.<sup>3,11,12,18-24</sup> Buildup of negative charge on insulating mask sidewalls by isotropic electrons is thought to deflect positive ion trajectories toward trench sidewalls (Fig. 2). Recently the effects of mask charging on ion directionality and feature profile evolution have been modeled. Hwang and Giapis have reported numerical simulations of etched profiles during high-density  $\text{Cl}_2$  plasma etching of Si.<sup>22</sup> Simulations with 0.1 and  $0.5 \mu\text{m}$  high masks showed that microtrench formation was aggravated when mask charging was included, and was worse for

<sup>a)</sup>Electronic mail: kbogart@lucent.com

## BEST AVAILABLE COPY

198

Bogart et al.: Mask charging and profile evolution

198

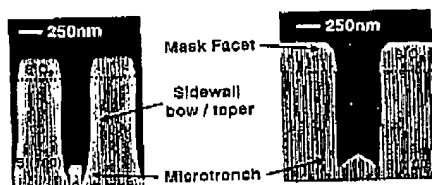


FIG. 1. Examples of anomalous feature profiles for  $\text{SiO}_2$ -masked  $\text{Si}(100)$  wafers.

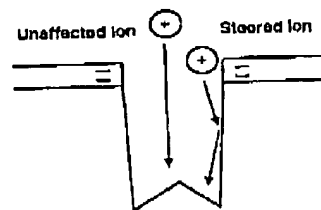


FIG. 2. Ion steering caused by mask charging.

higher aspect ratio trenches and high electron temperatures (8 eV). Schaepkens and Oehrlein have shown experimentally in  $\text{SiO}_2$  etching that charging of the insulating material enhances microtrench formation. A weak magnetic field increased the negative charge buildup on the oxide sidewall, thus steering positive ions towards one side of the trench and producing asymmetric microtrenches.<sup>24</sup>

This laboratory has produced several experimental investigations on the effect of high-density  $\text{Cl}_2$  plasma etching conditions on feature profile evolution in  $\text{SiO}_2$  patterned  $\text{Si}(100)$  and poly-Si.<sup>9,10</sup> In general, the microtrench depth increased with rf source power and decreased with rf substrate bias power. Increasing pressure changed the shape of microtrenches from broad wedge-shaped microtrenches to deep grooves. The sidewall contour influenced the microtrench shape, consistent with a mechanism in which ions are directed towards trench sidewalls, are scattered, and are subsequently focused to form microtrenches. The variety of sidewall contours and microtrench shapes with different plasma conditions suggests that the initial deflection of ions was variable, but did not clarify whether the IAD or mask charging was the primary cause.

In this study, we investigate the contribution of mask charging to ion deflection towards the sidewall and subsequent microtrench formation by etching  $\text{Si}(100)$  and poly-Si in  $\text{Cl}_2$  plasmas using both insulating and conductive mask materials.<sup>12</sup> Comparisons of etched profiles were made for insulating  $\text{SiO}_2$ -masked and for conductive, maskless (patterned Si only) wafers etched with several ion densities ( $n_i^+$ ) and ion energies ( $E_i^+$ ). Wafers patterned with conductive tungsten (W) masks were also etched with one set of plasma conditions. The results presented below show that charging of the insulating mask material is not a significant contribution to the formation of microtrenches or sidewall anomalies under typical conditions for  $\text{Cl}_2$  plasma etching of Si.

## II. EXPERIMENTAL METHODS

### A. High-density plasma reactor

The LAM TCP 9400SE™ high-density plasma etching system used to fabricate the conductive maskless wafers (described below in Sec. II B) and to etch all of the sample wafers has been described in detail previously.<sup>9,10</sup> The source and substrate bias rf powers were controlled separately, therefore  $n_i^+$  and  $E_i^+$  were independently varied. The plasma conditions used in this study to etch wafers masked with both insulating and conductive materials are listed in Table I.

### B. Wafer preparation

$\text{Si}(100)$  wafers (150 mm) with 7.5  $\mu\text{m}$  epitaxially grown silicon ( $p^+$ , 0.006–0.10  $\Omega\text{cm}$ ) were used as substrates. Undoped poly-Si (10 000 Å) deposited onto 1000 Å  $\text{SiO}_2$  and thermally annealed was also used as a substrate. Three different types of masked Si wafers were fabricated ( $\text{SiO}_2$ , maskless, and W) and their effect on etched profiles were compared. The  $\text{SiO}_2$  mask material was 5000 Å of plasma enhanced tetraethoxysilane (PETEOS) patterned using standard photolithography and etching techniques.<sup>9,10</sup> The pattern structure consisted of a repeating series of nested lines, nested trenches, isolated trenches, and isolated lines with nominal feature sizes from 0.17 to 0.60  $\mu\text{m}$ .<sup>9,10,25</sup> The patterned  $\text{SiO}_2$  mask [Fig. 3(a)] had flat tops, sharp corners, and tapered (83°) sidewalls. The underlying Si was then etched in the  $\text{Cl}_2$  plasmas described in Table I.

The conductive, "maskless" Si wafers were prepared by first etching  $\text{SiO}_2$ -masked wafers in a HBr plasma for 270 s. This produced ~1.5  $\mu\text{m}$  deep Si trenches with straight sidewalls and flat bottoms. The isolated lines had straight sidewalls and broad, shallow depressions at the base of the sidewalls, as reported previously.<sup>9,25</sup> Despite a  $\text{SiO}_2$  mask sidewall tapered at 83°, the postetching silicon sidewall

TABLE I. Experimental conditions, Langmuir probe results, and calculated angles for chlorine etching of  $\text{SiO}_2$ -masked  $\text{Si}(100)$ .

Plasma condition	TCP (W)	Bias (W)	$\text{Cl}_2$ flow (sccm)	Pressure (mTorr)	Etch time (s)	$E_i^+$ (eV)	$n_i^+$ ( $\times 10^{10}\text{ cm}^{-3}$ )	$T_e$ (eV)	$\theta_{\text{LAP}}$ (deg)	$\Delta\theta$ (deg)
Baseline	250	150	80	10	240	174	$3.83 \pm 0.24$	$1.97 \pm 0.01$	3.1	0.41
High TCP	500	150	80	10	140	124	$9.51 \pm 0.45$	$1.88 \pm 0.03$	3.6	0.58
High bias	250	250	80	10	200	241	$3.88 \pm 0.24$	$2.02 \pm 0.02$	2.6	0.30
Low pressure	250	150	80	2	200	135	$4.91 \pm 0.37$	$2.45 \pm 0.02$	3.9	0.53
Very low bias	750	25	80	10	270	24	$20.4 \pm 4.9$	$1.90 \pm 0.02$	8.3	3.0

## BEST AVAILABLE COPY

199

Bogart et al.: Mask charging and profile evolution

199

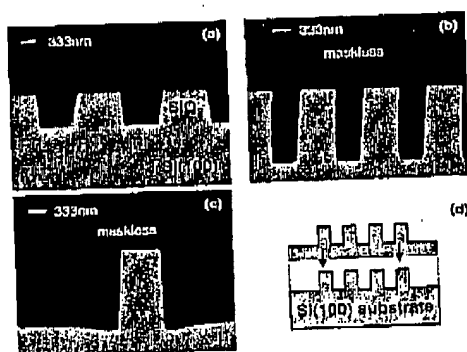


FIG. 3. SEM cross sections of (a) a  $\text{SiO}_2$  mask prior to experimental  $\text{Cl}_2$  plasma etching, (b)  $\text{Si}(100)$  maskless nested trenches after etching with  $\text{HBr}$  plasma and removal of the  $\text{SiO}_2$  mask, (c)  $\text{Si}(100)$  maskless isolated lines after etching with  $\text{HBr}$  plasma and removal of the  $\text{SiO}_2$  mask, and (d) a representation of pattern transfer for maskless samples etched in  $\text{Cl}_2$  plasma.

angle was  $-90^\circ$ . The  $\text{SiO}_2$  mask was removed in a 7:1 buffered oxide wet etch bath, leaving trenches and lines in the silicon. The bottoms of the trenches and the tops of the lines were flat, the sidewalls of the trenches were straight, and the corners of the lines were square [Fig. 3(b)]. The maskless isolated lines retained flat line tops, straight sidewalls, and the shallow depression adjacent to the sidewalls [Fig. 3(c)]. The maskless wafers were then etched with the same chlorine plasma conditions as the  $\text{SiO}_2$  masked samples (Table I) and the pattern was propagated down into the silicon wafer while allowing the individual etching characteristics for each plasma condition to evolve. The etch rates at the top of the silicon line and the bottom of the trench were essentially the same, thus, the initial trench depth was conserved during the etching process [Fig. 3(d)].

Wafers were also prepared using W as a mask material. A 5000 Å W/400 Å TiN (etch stop layer) stack was deposited onto  $\text{Si}(100)$  wafers. The pattern structure was etched into the W with a  $\text{SF}_6$  plasma, using a photoresist mask. The resulting W mask had slightly bowed sidewalls, rounded corners, and rough tops. The  $\text{Si}(100)$  surface was slightly roughened when the  $\text{SF}_6$  plasma broke through the TiN etch stop. The W-masked wafers were etched with the baseline plasma condition (Table I).

### C. Morphological analysis

The profiles of the etched features were analyzed using a Topcon DS-130C scanning electron microscope (SEM) with a Printerface Plus (GW Electronics) digital imaging system. The wafers were cleaved perpendicular to the trench direction and analyzed without metal sputter coating. Much of the data presented below consists of SEM micrographs. The terms used to describe feature profiles seen in the micrographs have been defined previously.<sup>9</sup> For lines or trenches, a straight sidewall has no curvature and is  $90^\circ$  to the surface plane of the wafer. A tapered sidewall is without curvature

TABLE II. Langmuir probe results for  $\text{Cl}_2$  etching of blanket  $\text{Si}(100)$ , blanket  $\text{SiO}_2$ , and  $\text{SiO}_2$ -masked  $\text{Si}(100)$  wafers. The results for the masked wafers are also shown in Table I.

Material	Pressure (mTorr)	rf source (W)	rf bias (V)	$n_e^{\text{max}}$ ( $\times 10^{16} \text{ cm}^{-3}$ )	$T_e$ (eV)
$\text{Si}(100)$	2	250	150	$4.22 \pm 0.27$	$2.38 \pm 0.02$
	10	250	150	$2.78 \pm 0.21$	$1.94 \pm 0.04$
	10	250	250	$2.83 \pm 0.37$	$1.98 \pm 0.01$
	10	500	150	$6.09 \pm 0.33$	$1.94 \pm 0.02$
	10	500	250	$5.53 \pm 0.15$	$1.96 \pm 0.03$
	10	750	25	$16.6 \pm 1.2$	$1.87 \pm 0.01$
$\text{SiO}_2$	2	250	150	$4.73 \pm 0.38$	$2.53 \pm 0.02$
	10	250	150	$2.87 \pm 0.61$	$2.02 \pm 0.02$
	10	250	250	$3.36 \pm 0.28$	$2.07 \pm 0.03$
	10	500	150	$7.43 \pm 0.26$	$2.04 \pm 0.04$
	10	500	250	$6.57 \pm 0.18$	$2.07 \pm 0.02$
	10	750	25	$19.2 \pm 4.5$	$1.94 \pm 0.03$
Masked	2	250	150	$4.91 \pm 0.37$	$2.45 \pm 0.02$
	10	250	150	$3.83 \pm 0.24$	$1.97 \pm 0.01$
	10	250	250	$3.88 \pm 0.62$	$2.02 \pm 0.02$
	10	500	150	$9.51 \pm 0.45$	$1.88 \pm 0.03$
	10	500	250	$9.62 \pm 0.35$	$1.90 \pm 0.01$
	10	750	25	$20.4 \pm 4.9$	$1.90 \pm 0.02$

and deviates from  $90^\circ$ . A bowed sidewall is curved away from the top of the line or mask. A microtrench is defined as the area etched away below the horizontal position of the center of the trench bottom. Unless otherwise specified, nominally  $0.6 \mu\text{m}$  wide features are shown.

### D. Langmuir probe and dc bias measurements

Positive ion densities and electron temperatures were measured with a Langmuir probe (Scientific Systems Smart-probe), described elsewhere.<sup>26,27</sup>  $\text{Si}(100)$ ,  $\text{SiO}_2$ , and  $\text{SiO}_2$ -masked wafers were used as substrates. Laframboise analysis was used to interpret the shapes of the current-voltage ( $I$ - $V$ ) curves. A reference electrode on the probe was used to correct the  $I$ - $V$  curves to shift the plasma potential during acquisition of the  $I$ - $V$  curves. The plasma potential ( $V_{pp}$ ) was 13–16 V at 10 mTorr and was consistently higher, 17–18 V, at 2 mTorr. The results taken with all three materials are listed in Table II.

Peak-to-peak rf voltages ( $V_{pp}$ ) on the substrate stage of a nominally identical plasma etching system (LAM 9600 PTX) were measured with a high voltage probe assembly supplied by LAM Research. As discussed below, the dc bias voltage ( $V_{dc}$ ) and the average  $E_i^+$  were estimated to be equal to  $V_{pp}/2$ .

## III. RESULTS

Changes in source rf and substrate bias rf powers or pressure will alter neutral and ion densities, ion energies, and ion angular distributions.<sup>1,14</sup> These alterations may also affect ion trajectories through differential charging of insulating mask materials. The results presented below address the charging issue by comparing  $\text{SiO}_2$ - and W-masked and maskless wafers etched under typical manufacturing plasma

BEST AVAILABLE COPY

TABLE III. Observations and measurements of silicon profiles etched with SiO<sub>2</sub>, maskless, and tungsten mask materials.

Mask material and plasma condition	Sidewall contour	$\mu$ -trench shape	Depth center (Å)	Etching rate (Å/s)	Depth $\mu$ -trench (Å)	Mask undercut	Mask etching rate (Å/s)	Selectivity	Mask facet angles (deg)
SiO <sub>2</sub> mask									
Baseline	Bow	Groove	8 500	60.7	10 000	None	7.1	8.5	None
500 W source	Bow	Groove	12 506	90.0	15 347	None	10.9	8.3	53
250 W bias	Bow	Groove	14 547	72.7	17 526	None	5.7	12.8	Rounded
2 mTorr	Taper	Wedge	9 625	48.1	10 875	Slight	8.1	5.9	46
750 W source	Taper	Groove	16 650	61.7	...	None	3.3	19	Rounded
Maskless									
Baseline	Bow	Groove	14 750	...	16 250	...	...	...	None
500 W source	Bow	Groove	16 983	...	18 981	...	...	...	50
250 W bias	Bow	Groove	17 629	...	20 176	...	...	...	57
2 mTorr	Taper	Wedge	15 984	...	17 150	...	...	...	47
Poly-Si	Taper	Wedge	5 524	...	6 423	...	...	...	42
750 W source	Taper	Groove	20 492	...	...	...	...	...	None
W mask									
Baseline	Bow	Groove	8 375	59.8	9 250	None	8.9	6.7	None

conditions used with the LAM 9400SE. Additionally, wafers were etched with conditions that would exacerbate the effect of mask charging (a high TCP source and very low substrate rf bias powers) to further test the effect of differential mask charging. A compilation of measurements and observations of shapes and dimensions, etching rates, and selectivities from resultant feature profiles for all the plasma conditions investigated is listed in Table III.

#### A. Baseline plasma condition

Nested trenches for SiO<sub>2</sub>-masked Si(100) wafers etched with the baseline condition (Table I) are shown in Fig. 4(a). The sidewalls of the trench are bowed with an inflection point near the bottom of the trench. Sharp, groove-shaped microtrenches are observed at the outer edges of the trench bottom and the center area of the trench is smooth and round, without definite planes. No undercutting at the Si/SiO<sub>2</sub> interface is observed. The top corners of the mask are slightly

rounded, but not faceted. The angle of the mask with respect to the surface normal is  $\sim 83^\circ$ , and did not change with etching.

Nested trenches on maskless wafers etched with the baseline condition are shown in Fig. 4(b). The overall trench profile and microtrenches obtained with a conductive material are similar to those produced with an insulating mask. The trenches also have bowed sidewalls with an inflection point close to the trench bottom. Sharp, groove-shaped microtrenches are observed at the edges of the trench bottom and the center is round without well-defined planes. The top corner of the trench sidewall (silicon) is not faceted, but is slightly rounded. If charging of the insulating mask were the primary cause of microtrench formation, we would expect the features etched with a conductive "silicon mask" to be devoid of microtrenches.

Isolated lines etched with the baseline condition [Figs. 4(c) and 4(d)] exhibit nearly identical sidewall contours as the nested trenches [Figs. 4(a) and 4(b)] for SiO<sub>2</sub>-masked and maskless wafers, respectively. The microtrenches adjacent to the bottom of the line are similar in shape and severity to those observed inside the nested trenches. The shape of the SiO<sub>2</sub> mask and the tops of the maskless line are also the same as those of the nested trenches.

There are subtle differences between the contours of the trenches and lines etched with different mask materials that we attribute to effects other than mask charging. In the maskless samples, the sidewalls of nested trenches and isolated lines flare away towards the trench center or the open area, relative to the SiO<sub>2</sub>-masked samples. Before etching, the SiO<sub>2</sub> mask sidewalls (5000 Å high) are tapered ( $83^\circ$ ) and the maskless line sidewalls (15 000 Å high) are straight, ion impact and subsequent scatter from the different materials, angles, and aspect ratios may account for the minor differences between the feature profiles. The most noticeable difference between the SiO<sub>2</sub>-masked and maskless samples is

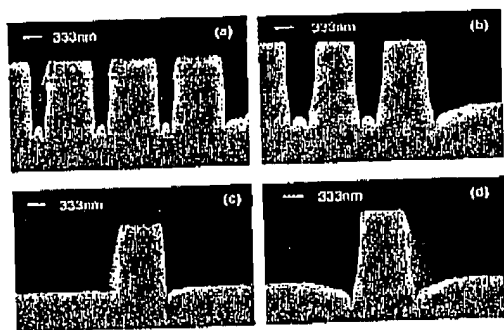


FIG. 4. SEM cross sections of Si(100) etched with the baseline plasma condition (Table I) for (a) SiO<sub>2</sub>-masked nested trenches, (b) maskless nested trenches, (c) a SiO<sub>2</sub>-masked isolated line, and (d) a maskless isolated line.

BEST AVAILABLE COPY

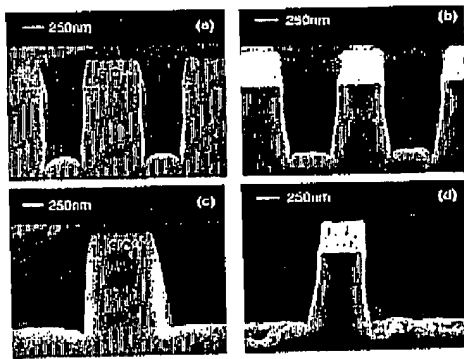


FIG. 5. SEM cross sections of Si(100) etched with the baseline plasma condition (Table I) for 145 s for (a) SiO<sub>2</sub>-masked nested trenches, (b) maskless nested trenches, (c) a SiO<sub>2</sub>-masked Si(100) isolated line, and (d) a W-masked isolated line.

that the microtrench adjacent to the maskless isolated line has an additional declivity towards the open area.<sup>25</sup> This declivity originates from the broad, shallow depression formed during the HBr etch [Fig. 3(c)]. The Cl<sub>2</sub> plasma etch may exacerbate the depth of this area through ion-induced etching yields that peak at off-normal incidence.<sup>28–30</sup> Taking the initial declivity into account [Fig. 3(c)], the similarity of the microtrench shapes with both insulating and conductive materials, and thus with and without the possibility of charge-induced deflection of ions, suggests that mask charging is not a major influence under these conditions.

### B. Tungsten mask

In the results presented above, the absence of a mask material with greater etch selectivity than the underlying silicon might be thought to affect the profile evolution and the mask charging experiment. To address this issue, we fabricated Si(100) wafers patterned with a conductive tungsten mask, and then etched them with the baseline condition (Table I). The W mask was the same thickness as the SiO<sub>2</sub> mask, allowing the initial aspect ratios to be more similar than those of the maskless samples. Other complications make a direct comparison more difficult. The initial W mask profile was rough on top and had slightly bowed sidewalls. As noted above, the etch-stop layer was penetrated by the SF<sub>6</sub> plasma during the W mask etch and resulted in roughening of the Si surface prior to Cl<sub>2</sub> plasma etching. The morphology of this surface is propagated during the Cl<sub>2</sub> plasma etch, making the microtrenches more difficult to discern.

The W-masked nested trench profile [Fig. 5(b)] is comparable to its SiO<sub>2</sub>-masked counterpart [Fig. 5(a), etched for the same time, 145 s] and to the maskless sample [Fig. 4(b)], in that it has bowed sidewalls, groove-shaped microtrenches, and rounded trench bottoms. No undercut was observed with the W mask, and the top of the W mask is not faceted, but is slightly rounded and smoother after Cl<sub>2</sub> plasma exposure.

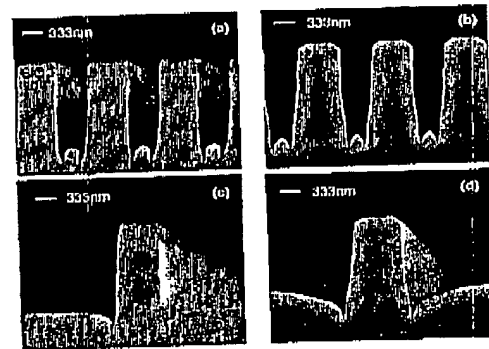


FIG. 6. SEM cross sections of Si(100) etched with high (500 W, Table I) TCP source power for (a) SiO<sub>2</sub>-masked nested trenches, (b) maskless nested trenches, (c) a SiO<sub>2</sub>-masked isolated line, and (d) a maskless isolated line.

The corresponding isolated lines [Figs. 5(c), SiO<sub>2</sub> masked and 5(d), maskless] are virtually identical to their nested counterparts. The microtrenches with the W-masked samples are approximately half as deep as those formed with the SiO<sub>2</sub> mask. This variation in microtrench severity is likely a result of the slight extension of W mask material from the bowed sidewall at the W-Si interface. Si etching adjacent to the W sidewall will be inhibited during the first part of the etch by this masking effect, and will slow the microtrench formation rate until the W material is etched away. Shallower microtrenches would be produced. Modest changes in the ion scattering mechanism from materials of differing mass and from mask sidewalls with slightly different shapes may also affect the etching process.<sup>8</sup> The feature profile results from the W-masked wafers are qualitatively comparable to those of maskless wafers and wafers masked with SiO<sub>2</sub>, indicating that differential mask charging is not the cause of microtrench formation. The shallower microtrenches produced with the W mask can be explained without having to evoke mask charging arguments.

### C. Increased rf source power

The rf source power was doubled from 250 to 500 W. Profiles for nested trenches etched with the SiO<sub>2</sub> mask are shown in Fig. 6(a). In contrast to the baseline condition, the microtrenches are deeper (greater overall etch depth for this condition) and curve towards the trench center. The trench sidewalls are bowed, with the curved contour extending underneath the SiO<sub>2</sub> mask, giving the sidewalls a slight "hour-glass" shape. The trench bottom is not rounded, but has two distinct planes, that form a polygonal shape in the center of the trench. With the higher rf source power, the SiO<sub>2</sub> mask was slightly faceted. No undercutting directly below the Si/SiO<sub>2</sub> interface is observed.

Maskless wafers etched with the high rf source power [Fig. 6(b)] have trench sidewall contours and microtrenches comparable to those etched with the insulating SiO<sub>2</sub> mask [Fig. 6(a)]. The trench sidewalls are bowed their entire

## BEST AVAILABLE COPY

length with an inflection point near the bottom of the sidewall, deep groove-shaped microtrenches curve towards the center of the trench, and the trench bottom has two distinct planes, that form a point in the bottom of the trench. The microtrenches in the maskless sample are shallower than those in the  $\text{SiO}_2$ -masked sample. The smaller microtrench size and the more triangular trench bottom shape with the maskless sample are likely due to slight changes in ion reflection from the differently angled sidewalls and the shorter trench width near the bottom of the trench. The tops of the maskless trench sidewalls are faceted when etched at higher rf source power.

Isolated lines etched with high TCP power [Figs. 6(c) and 6(d)] are also presented for  $\text{SiO}_2$ -masked and maskless wafers, respectively. The overall sidewall contours and the tops of the lines ( $\text{SiO}_2$  masked and maskless) are near replicas of the nested trenches. The maskless sample has the additional declivity away from the isolated line, an enlargement of the depression generated by the initial HBr plasma etch [Fig. 3(c)]. With the initial maskless contour taken into account, the shapes and depths of the microtrenches are similar with and without an insulating mask.

Slight differences between the etched profiles are noticeable for  $\text{SiO}_2$ -masked and maskless samples and are potentially due to variations in ion scattering mechanisms from the different mask materials and mask shapes, as mentioned above, and not due to the effects of mask charging. At the higher TCP power, the sidewall contour for the  $\text{SiO}_2$ -masked nested trenches is more bowed, having more of an hourglass shape, than for the corresponding isolated lines. A likely explanation is that scattering of ions from adjacent features in nested regions leads to a slight erosion of the sidewalls. This nearest neighbor effect may also form the inflection points, seen only in nested trenches.<sup>23</sup> It is important to note, however, that ion scattering from these adjacent features does not lead to microtrench formation, since microtrenches are observed with isolated lines. The isolated lines provide a superior test of the mask charging effect than do the nested features because scattering from adjacent trench sidewalls cannot contribute to the profile shape.

Langmuir probe measurements obtained during  $\text{Cl}_2$  plasma etching of a Si(100) wafer revealed that as rf source power was increased from 250 to 500 W,  $n_i^+$  increased from  $3.83 \pm 0.24 \times 10^{10}$  to  $9.51 \pm 0.45 \times 10^{10} \text{ cm}^{-3}$  and  $T_e$  decreased slightly, from  $1.97 \pm 0.01$  to  $1.88 \pm 0.03 \text{ eV}$ . With the increase in rf source power,  $V_{dc}$  changed from  $-165$  to  $-120 \text{ V}$ . The feature profiles etched at 500 W show a marked increase in the degree of the sidewall bow, the depth of the microtrenches, and the formation of facets on the tops of both the  $\text{SiO}_2$  and maskless (silicon) trenches relative to those etched with the baseline condition (250 W). These data suggest that an increase in  $n_i^+$ , and hence ion flux, worsens microtrench and facet formation. The presence of an insulating mask material, however, does not cause a significant change in the overall feature profile for plasma conditions with high ion flux.

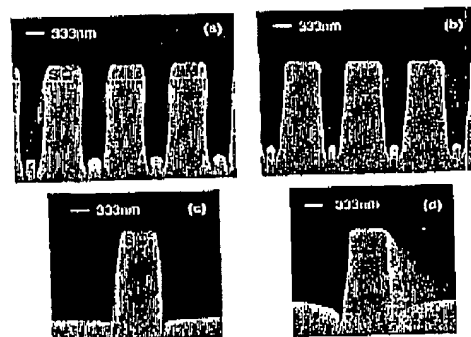


Fig. 7. SEM cross sections of Si(100) etched with high (250 W, Table I) of substrate bias power for (a)  $\text{SiO}_2$ -masked nested trenches, (b) maskless nested trenches, (c) a  $\text{SiO}_2$ -masked isolated line, and (d) a maskless isolated line.

#### D. Increased substrate rf bias power

The substrate rf bias power was increased to 250 W relative to the baseline condition (150 W). Nested trenches masked with  $\text{SiO}_2$  and etched with this condition are shown in Fig. 7(a). The sidewalls of the trench are significantly more bowed than samples etched with the baseline or high TCP source power conditions, resulting in a more hourglass-like shape. Deep groove-shaped microtrenches are observed at the edge of the trench sidewalls, and they curve towards the trench center. The interior side of the microtrench is vertical and the trench center is flat, with rounded edges. No undercutting directly below the Si/SiO<sub>2</sub> interface is observed and the  $\text{SiO}_2$  mask is slightly faceted.

The maskless wafers etched with high rf substrate power are nearly identical to their  $\text{SiO}_2$ -masked counterparts. The trench sidewalls are bowed, with an inflection point near the bottom of the trench [Fig. 7(b)]. Deep groove-shaped microtrenches curve towards the center of the trench, which has two distinct planes, forming a polygonal shape. The difference in the polygonal shapes in the center of the  $\text{SiO}_2$ -masked and maskless trenches may be from differences in the scattering angle for ions scattering from the smoothly curved  $\text{SiO}_2$ -masked sidewall and the inflection point in the maskless sidewall. The tops of the maskless trenches are slightly faceted.

The isolated lines for these plasma conditions [Figs. 7(c),  $\text{SiO}_2$ -masked and 7(d), maskless] are similar to the nested features with respect to the degree and overall shape of the microtrenches. As was observed with the high source power condition (Sec. III B), sidewalls of the  $\text{SiO}_2$ -masked nested lines are more bowed than the isolated lines (which are nearly straight) as expected if this attribute is caused by ion scattering from adjacent features. The maskless isolated line shows the declivity away from the line, initiated by the HBr etch, and not due to mask charging effects.

Increased rf power to the wafer substrate increased the sheath potential ( $V_{dc}$  changed from  $-165$  to  $-230 \text{ V}$ ), thus

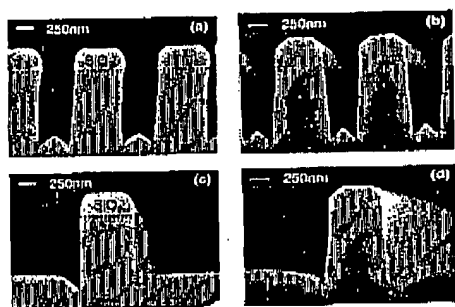


FIG. 8. SEM cross sections of Si(100) etched with low pressure (2 mTorr, Table I) for (a) SiO<sub>2</sub>-masked nested trenches, (b) maskless nested trenches, (c) a SiO<sub>2</sub>-masked isolated line, and (d) a maskless isolated line.

increasing  $E_f^+$  and decreasing the width of the IAD<sup>14,15</sup> (see the discussion below). Greater substrate bias potential had little effect on  $n_i^+$  ( $3.88 \pm 0.62 \times 10^{10} \text{ cm}^{-3}$ ) or on  $T_e$  ( $2.02 \pm 0.02 \text{ eV}$ ) relative to the values at 150 W rf bias power mentioned above (Table I). The trench profiles etched at higher substrate bias power (250 W) have a more severe sidewall bow and deeper microtrenches than their baseline condition counterparts, and are similar to the trenches etched with high rf source power. The tops of the maskless trenches and lines were slightly faceted, more so than the trenches etched at 150 W, but less than the trenches etched at 500 W source power. Deeper microtrenches were formed with a greater  $E_f^+$  than with the baseline condition or with a twofold increase in  $n_i^+$ , suggesting that ion energy has a strong effect on microtrench development. However, at high  $E_f^+$ , the overall profile of features etched with SiO<sub>2</sub>-masked and maskless wafers is the same, thus mask charging is not a factor in profile evolution.

### E. Decreased pressure

The gas pressure was decreased from 10 to 2 mTorr and the overall effect on the etched trench profile was dramatic. For the SiO<sub>2</sub>-masked wafers, the nested trench sidewalls were tapered [Fig. 8(a)], contrasting with the bowed contours observed with the baseline, high TCP source and high substrate bias power conditions. The microtrench shape is strikingly different, consisting of a broad wedge that originates at the sidewall and overlaps to form a point at the center of the trench. In contrast with the samples described in Secs. III A, III B, and III C, the top of the SiO<sub>2</sub> mask has extensive facets and the silicon sidewall is slightly undercut below the SiO<sub>2</sub> mask.

The corresponding nested trenches for the maskless wafers etched with low pressure are shown in Fig. 8(b) and are comparable to trenches etched with the insulating SiO<sub>2</sub> mask, indicating that mask charging is also not the fundamental cause of microtrenches at low pressures. The maskless nested trenches have tapered sidewalls with a slight inflection point towards the bottom of the trench. The

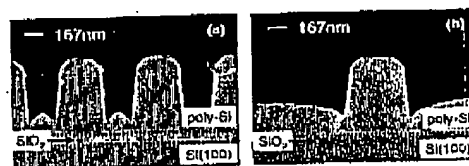


FIG. 9. SEM cross sections of poly-Si etched with low pressure (2 mTorr, Table I) for (a) maskless nested trenches and (b) a maskless isolated line.

microtrench is broad and has two distinct planes that overlap to form a point at the center of the trench. The tops of the silicon lines are extensively faceted.

The isolated lines shown in Figs. 8(c) (SiO<sub>2</sub>-masked) and 8(d) (maskless) are nearly identical to the nested trenches taking into account the shallow depression in the maskless sample created by the HBr etch [Fig. 3(c)]. The undercut present in the SiO<sub>2</sub>-masked nested trenches is not present in the isolated line. This suggests that ion scattering from the facets at the top of the nearest neighbor line is the source of the undercut.

The angles from the water surface of the microtrench planes and facet planes in Fig. 8 are strikingly similar. The facets at the top of etched lines form at low pressure when the ion-induced etching yield peaks at off-normal angles ( $\sim 40^\circ$ – $60^\circ$ ).<sup>25</sup> The same mechanism is likely contributing to the well-defined plane angles within the microtrenches.

Langmuir probe measurements at 2 mTorr Cl<sub>2</sub> indicated that both  $n_i^+$  ( $4.91 \pm 0.37 \times 10^{10} \text{ cm}^{-3}$ ) and  $T_e$  ( $2.45 \pm 0.02 \text{ eV}$ ) increased at 2 mTorr relative to the 10 mTorr baseline condition. Conversely, the ion energy decreased, compared to the baseline condition ( $V_{dc}$  changed from  $-165$  to  $-130 \text{ V}$ ). At lower pressures, the IAD is likely to increase.<sup>14</sup> This may explain the extensive broadening of the microtrench etched at 2 mTorr. The higher ion flux and lower total neutral flux at 2 mTorr may increase the sputtering component<sup>31</sup> relative to the chemically enhanced etching component.<sup>28,30</sup> This could explain the formation of large facets at the tops of the trenches for both the SiO<sub>2</sub>-masked and maskless wafers [Figs. 8(a) and 8(b), respectively] in addition to the well-defined planes in the broad microtrenches. Despite the extensive differences in the trench profiles between the 2 mTorr and baseline (10 mTorr) conditions, the presence of an insulating mask does not significantly alter the overall contours of the etched feature.

Differential charging of insulating and conductive materials is also a concern for etching poly-Si. Maskless wafers were also prepared with undoped poly-Si (Sec. II B) and then etched at 2 mTorr [Figs. 9(a), nested trenches and 9(b), isolated line, nominally  $0.35 \mu\text{m}$ ]. Etching was stopped before reaching the buried SiO<sub>2</sub> to avoid the complicating effects of charge-induced notching,<sup>32–34</sup> thus resulting in a smaller aspect ratio. The profiles etched into poly-Si were virtually identical to those found with Si(100),<sup>25</sup> indicating that crystallographic-specific etching of Si(100) in Cl<sub>2</sub> plasmas does not occur, and that the presence of an insulating SiO<sub>2</sub> subsurface layer has no effect on mask charging prior to

## BEST AVAILABLE COPY

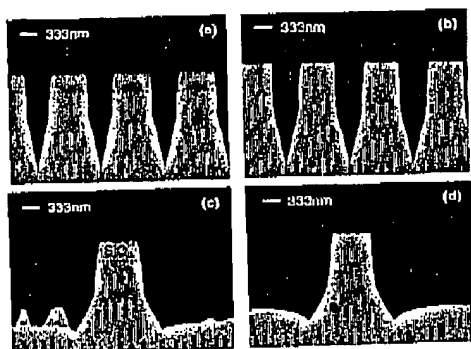


FIG. 10. SEM cross sections of Si(100) etched with high (750 W) TCP power and very low (25 W, Table I) bias power for (a) SiO<sub>2</sub>-masked nested trenches, (b) maskless nested trenches, (c) SiO<sub>2</sub>-masked isolated lines, and (d) maskless isolated lines. Micromasking is present in the open areas of the SiO<sub>2</sub>-masked isolated line.

etching completely through the poly-Si layer.

#### F. High rf power and very low substrate bias

The plasma conditions explored above represent roughly twofold deviations in rf powers from the optimal operating conditions for poly-Si gate etching with a Cl<sub>2</sub>/HBr plasma.<sup>33</sup> Under these conditions, no significant differences in the etched feature profiles were observed with insulating or conductive mask materials. To better test whether mask charging affects profile evolution, we etched SiO<sub>2</sub>-masked and maskless wafers with high (750 W) rf source power and very low (19–25 W) rf substrate bias. As will be shown below, these conditions will maximize any possible effect of mask sidewall charging through increased  $n_i^+$  (increased ion flux to sidewalls) and substantially decreased  $E_i^+$  (increased IAD). Nested trenches for SiO<sub>2</sub>-masked and maskless wafers etched in the extreme conditions are shown in Figs. 10(a) and 10(b), respectively. The trench sidewalls for both samples are straight for the top one third and severely tapered for the bottom two thirds. The bottom of the trench is a single V-shaped groove, resulting from overlap of microtrenches. The SiO<sub>2</sub> mask is rounded at the top and no undercut is observed. The top corners of the maskless lines are square and without facets.

The SiO<sub>2</sub>-masked and maskless isolated lines etched with these extreme conditions are shown in Figs. 10(c) and 10(d), respectively. The sidewall contour, trench bottom, and line tops are nearly identical to each other and to the nested trenches etched with the same plasma conditions [Figs. 10(a) and 10(b)]. Adjacent to the isolated lines is a broad microtrench that gradually slopes upward to the open area for both SiO<sub>2</sub>-masked and maskless samples. Some micromasking is observed in the open area near the SiO<sub>2</sub>-masked isolated lines [Fig. 10(c)], but it was not present in the maskless wafer. The greater depth of the maskless microtrench can be attributed to the initial shallow depression formed during the

HBr etch. The etched profiles for the insulating and conductive materials are virtually indistinguishable. The data in Fig. 10 are the strongest evidence of all the conditions investigated that mask charging is unimportant in profile evolution and microtrench formation.

These plasma conditions increase  $n_i^+$  to  $2.04 \pm 0.49 \times 10^{11} \text{ cm}^{-3}$  and decrease  $E_i^+$  to 30 eV, producing a relatively large IAD. The effect of mask charging should be exacerbated by the low  $E_i^+$  and by the broad IAD, however, the results clearly show that no significant difference is produced when using insulating or conducting mask materials under these conditions. While it is conceivable that mask charging could play a role in microtrench formation under these conditions, it will be shown below that the electric fields present on the sides of the SiO<sub>2</sub> mask would have to be larger than recent predictions to cause a significant deflection of ions relative to the expected IAD.

The Langmuir probe measurements of  $n_i^+$  and  $T_e$  taken with blanket Si(100), blanket SiO<sub>2</sub>, and SiO<sub>2</sub>-masked Si(100) wafers are listed in Table II. As expected,  $n_i^+$  increased with increased rf source power. No significant effect from increasing rf bias power was observed. The patterned wafers had the highest  $n_i^+$ , followed by SiO<sub>2</sub> and then Si(100), although the difference in  $n_i^+$  values was slight.  $T_e$  decreased slightly with increasing rf source power. Lower rf bias power produced slightly lower average  $T_e$  values, although the standard deviations of the averages overlap. The decrease in pressure produced a substantial increase in  $T_e$ , as expected. In general, the  $T_e$  values were largest for SiO<sub>2</sub> wafers, followed by SiO<sub>2</sub>-masked wafers, and Si(100) wafers had the lowest values, although the magnitude of the differences was small. The change in  $T_e$  with substrate material is likely a function of the amount of etching products produced during etching. SiO<sub>2</sub> is not readily etched in Cl<sub>2</sub> plasmas relative to Si and would not produce a high concentration of etching products. Large numbers of etching products, such as SiCl<sub>x</sub> ( $x=1, 2, 3$ ), however, will reduce  $T_e$  through increased gas phase collisions and lower ionization potentials.

#### IV. DISCUSSION

The data presented above are strong evidence that charging of insulating mask materials is not the primary cause of microtrench formation, nor does charging affect the overall contour of a trench or line sidewall. Therefore, the angular distribution of ions impacting and subsequently scattering from the etching feature are likely to be the primary cause of nonvertical sidewalls and microtrench formation.

We can estimate both the IAD in the plane parallel to the wafer and the added angle,  $\Delta\theta$ , that an ion would be deflected by a buildup of charge on the mask. The IAD is determined by the ratio of the ion velocity angular distribution on the presheath-sheath boundary ( $v_{ip}$ ) and the sheath potential ( $E_{sh}$ ), assuming a collisionless sheath,

## BEST AVAILABLE COPY

$$\theta_{\text{IAD}} = \arctan \left( \frac{v_{\parallel}}{\left( \frac{2E_{\text{sh}}}{m_i} \right)^{1/2}} \right) \quad (1)$$

where  $m_i$  is the average ion mass. Ions entering the presheath from the bulk plasma are at the gas temperature ( $T_g$ ). In the presheath, ions are accelerated by the ambipolar fields with energies  $\approx T_e/2$ . If ion-neutral collisions occur in the sheath, some of this energy will be transferred into translational motion parallel to the wafer, increasing the IAD. The spread in the IAD at the presheath sheath boundary can be characterized by a new ion "temperature,"  $T_i^{\text{sh}} \gg T_g$ . We can use  $T_i^{\text{sh}}$  to estimate  $v_{\parallel}$ ,

$$v_{\parallel} = \left( \frac{2T_i^{\text{sh}}}{m_i} \right)^{1/2} \quad (2)$$

and, therefore,

$$\theta_{\text{IAD}} = \arctan \left( \frac{T_i^{\text{sh}}}{E_{\text{sh}}} \right)^{1/2} \quad (3)$$

Ion temperatures on the order of 0.2–0.5 eV have been reported for the types of plasmas studied here.<sup>14,15,33</sup> Assuming that  $T_i^{\text{sh}} = 0.5$  eV at 10 mTorr and is independent of source and bias powers, we estimate  $\theta_{\text{IAD}}$  values ranging from 2.6° at the highest (250 W) bias power to 8.3° at the lowest (25 W) bias power, Table I. Assuming that  $T_i^{\text{sh}}$  scales with  $T_e$ , the  $\theta_{\text{IAD}}$  at 2 mTorr was computed with  $T_i^{\text{sh}} = 0.63$  eV. The relative changes in  $\theta_{\text{IAD}}$  at a constant pressure of 10 mTorr should be valid, but comparisons with the 2 mTorr condition are more uncertain.<sup>14,15</sup>

The  $\theta_{\text{IAD}}$  can also be estimated from the profiles in Figs. 10(c) and 10(d). The severe tapers starting approximately halfway down the isolated line sidewall in Figs. 10(c) and 10(d) can be explained by the loss of half of the IAD at the edge of the mask from shadowing. The angle between the surface normal and the line drawn from the top corner of the mask to the midpoint of the tapered portion of the sidewall can be used to obtain  $\theta_{\text{IAD}}$ . Our assumptions include a perfectly vertical mask and etched feature sidewalls and an angle-independent ion-induced etching yield, which is a reasonable assumption since the top corners of the features in Figs. 10(b) and 10(d) did not become faceted, although the estimate is subject to complications from microtrench formation. From Fig. 10,  $\theta_{\text{IAD}}$  is  $\sim 9^\circ$  for  $\text{SiO}_2$ -masked wafers and  $\sim 7^\circ$  for maskless samples, in good agreement with the value derived from Eq. (3) for the same plasma conditions (8.3°).

Negative charge on the side of the insulating mask will distort the angular distribution of ions impacting the sides and bottoms of etched features, depicted in Fig. 2. If we assume that ions near the mask experience an attractive transverse electric field,  $E_{\text{tr}}$ , over a length,  $l$ , then they will be deflected by an angle,  $\Delta\theta$ , approximated by

$$\Delta\theta = \arctan \left( \frac{eE_{\text{tr}}l}{2E_{\text{sh}}} \right) \quad (4)$$

It is very difficult to measure or compute  $E_{\text{tr}}$ , nonetheless, modeling studies have been reported.<sup>11,12,33,36</sup> Computing  $E_{\text{tr}}$  is made difficult by incomplete knowledge of the IAD and ion energy distribution, and the electron energy distribution function. In addition, the conductivity along the surface of insulating materials is believed to occur in plasmas from surface damage, deposition of weakly conducting materials, and creation of electron-hole pairs by ultraviolet (UV) radiation.<sup>37</sup> An average electric field of  $2 \times 10^5$  V/cm within  $\sim 0.125$   $\mu\text{m}$  of the mask sidewall is suggested from the potentials calculated by Hwang and Giapis<sup>33,36</sup> and by Sawin and co-workers.<sup>11</sup> Assuming a constant field over a length  $l = 0.125$   $\mu\text{m}$ ,  $\Delta\theta = 0.41^\circ$  is obtained for the baseline condition with  $E_{\text{tr}} = 174$  V. Calculated  $\Delta\theta$  values for the other plasma conditions explored are listed in Table I. With the exception of the high TCP source power, very low bias power condition, the calculated  $\Delta\theta$  are small compared to  $\theta_{\text{IAD}}$  (11%–16%). If the reported fields of  $2 \times 10^5$  V/cm near insulating masks, computed from charging models,<sup>11,12,33,36</sup> are approximately correct, then the lack of significant differences in profiles etched with and without insulating masks is not surprising. The field near the mask would have had to have been at least  $\sim 2$  times higher to cause observable effects.

In contrast,  $\Delta\theta$  for the very high TCP and very low substrate bias power condition is 3.0°, or 36% of the  $\theta_{\text{IAD}}$ . Under these conditions, ions would be expected to deflect towards the feature sidewalls. Increased ion flux to the sidewall would increase the severity of the sidewall bow and, concomitantly, increase the severity of microtrench formation and reduce the size of the tapered region of the sidewall. If microtrench formation was caused by mask charging, the most severe microtrenches would form with the  $\text{SiO}_2$ -masked wafer. However, the microtrenches adjacent to the isolated lines with the  $\text{SiO}_2$ -masked wafer are slightly smaller than those with the maskless wafer [Figs. 10(c) and 10(d), respectively]. If we assume that a 20% increase in  $\theta_{\text{IAD}}$  will produce an observable increase in microtrench severity ( $\Delta\theta = 1.6^\circ$  computed from  $eE_{\text{tr}}l = 1.1 \times 10^9$  V/cm), then the field near the insulating mask in our experiment must be much less than  $1 \times 10^5$  V/cm.

## V. CONCLUSION

We have clearly shown that charging of an insulating mask is not the primary origin of microtrench formation during  $\text{Cl}_2$  etching of Si(100) or poly-Si. While unique feature profiles were obtained as rf source and substrate rf bias powers and pressures were varied, for each of the plasma conditions similar feature profiles evolved whether the mask material was insulating  $\text{SiO}_2$ , conductive silicon (maskless), or W. Therefore, under conditions that are typically used to etch Si in  $\text{Cl}_2$  plasmas, buildup of negative charge on the sidewalls of insulating masks from the broad electron angular distribution and narrow IAD does not significantly affect feature profile evolution. From simple vector addition of the ion motion parallel to the wafer surface and the directed ion free fall through the sheath, we estimated the angular spread of

## BEST AVAILABLE COPY

206

Bogart et al.: Mask charging and profile evolution

206

ions impacting the wafer in the absence of mask charging to be  $2.6^\circ$  and  $8.3^\circ$  at the highest (241 eV) and lowest (24 eV) ion energies, respectively. Based on reported computed estimates of the electric field ( $2 \times 10^5$  V/cm) near charged, insulating masks, we calculated that ions would be deflected toward the mask by  $0.30^\circ$  and  $3.0^\circ$  at the highest and lowest  $E_i^+$ , respectively. At the highest  $E_i^+$ , such a small deflection would not be expected to produce a noticeable effect on etched profiles. At the lowest  $E_i^+$ , however, a deflection of  $\sim 36\%$  would be expected to alter the etched profile, but no change was observed. If a  $\Delta\theta$  of 20% is assumed to cause an observable change in the feature profile then, under these conditions, the electric field near the mask sidewall produced by mask charging could not have exceeded  $1 \times 10^5$  V/cm. In conclusion, feature profile evolution during  $\text{Cl}_2$  plasma etching of Si(100) and poly-Si is not affected by ion deflection due to mask charging, but is directed by the angular distribution of ions impacting and scattering from the evolving feature.

## ACKNOWLEDGMENTS

The authors gratefully thank the staff of the Silicon Fabrication Research Laboratory at Murray Hill for their assistance in fabrication of wafer samples and A. Kornblit, E. A. Reiman, and H. L. Maynard for helpful discussions.

- <sup>1</sup>M. A. Lieberman and A. J. Lichtenberg, *Principles of Plasma Discharges and Materials Processing* (Wiley, New York, 1994).
- <sup>2</sup>S. Wolf, *Silicon Processing for the VLSI Era* (Lattice Press, Sunset Beach, CA, 1990), Vol. II.
- <sup>3</sup>F. J. Dalton, J. C. Arnold, H. H. Sawin, S. Swan, and D. Cordiss, *J. Electrochem. Soc.* **140**, 2395 (1993).
- <sup>4</sup>R. A. Gottsche, C. W. Jurgensen, and D. J. Vitkavage, *J. Vac. Sci. Technol. B* **10**, 2133 (1992).
- <sup>5</sup>S. V. Nguyen, D. Dobuzinsky, S. R. Stiffler, and G. Chrisman, *J. Electrochem. Soc.* **138**, 1112 (1991).
- <sup>6</sup>S. Ohki, M. Oda, H. Akiya, and T. Shilain, *J. Vac. Sci. Technol. B* **5**, 1611 (1987).
- <sup>7</sup>M. Suto, K. Sakuma, and Y. Arima, *Proceedings of the 1985 Dry Process Symposium II, 24-25 October 1985* (Institute of Electrical Engineers of Japan, 1985), pp. 102-107.
- <sup>8</sup>R. J. Hoekstra, M. J. Kushner, V. Sukharev, and P. Schoenborn, *J. Vac. Sci. Technol. B* **16**, 2102 (1998).
- <sup>9</sup>J. M. Lane, F. P. Klemens, M. V. Malyshev, K. H. A. Bogart, and J. T. C. Lee, *J. Vac. Sci. Technol. A* (to be published).

- <sup>10</sup>M. A. Vyvada, H. Lee, M. V. Malyshev, F. P. Klemens, M. Canillo, V. M. Dannelly, D. B. Graves, A. Kornblit, and J. T. C. Lee, *J. Vac. Sci. Technol. A* **16**, 1 (1998).
- <sup>11</sup>A. P. Mahorwala, Doctoral thesis, Massachusetts Institute of Technology, 1998.
- <sup>12</sup>S. Murakawa and J. P. McVittie, *Jpn. J. Appl. Phys., Part 1* **33**, 2184 (1994).
- <sup>13</sup>A. C. Westerheim, A. H. Lahan, J. H. Dubush, J. C. Arnold, H. H. Sawin, and V. Y. Wang, *J. Vac. Sci. Technol. A* **13**, 833 (1995).
- <sup>14</sup>E. A. Aydil, B. O. M. Quinlan, J. T. C. Lee, J. A. Gregus, and R. A. Gottsche, *Solid-State Electron.* **42**, A75 (1998).
- <sup>15</sup>R. A. Gottsche, *J. Vac. Sci. Technol. B* **11**, 1884 (1993).
- <sup>16</sup>K. P. Giapis, T. A. Moore, and T. K. Minton, *J. Vac. Sci. Technol. A* **13**, 959 (1995).
- <sup>17</sup>G. S. Hwang, C. M. Anderson, M. J. Gordon, T. A. Moore, T. K. Minton, and K. P. Giapis, *Phys. Rev. Lett.* **77**, 3040 (1996).
- <sup>18</sup>A. P. Mahorwala, J. P. Chang, and H. H. Sawin (private communication, 1998).
- <sup>19</sup>T. Arikawa, K. Horioka, M. Sekine, H. Okano, and Y. Horiike, in Ref. 7, pp. 114-119.
- <sup>20</sup>J. C. Arnold and H. H. Sawin, *J. Appl. Phys.* **70**, 5314 (1991).
- <sup>21</sup>D. J. Eganman and R. C. Alkire, *J. Electrochem. Soc.* **135**, 941 (1988).
- <sup>22</sup>G. S. Hwang and K. P. Giapis, *Mask Charging Effects on Feature Profile Evolution During High-Density Plasma Etching*, San Diego, CA, 1998 (The Electrochemical Society, Pennington, NJ, 1998), pp. 66-70.
- <sup>23</sup>G. S. Oehrlein, *Surf. Sci.* **386**, 222 (1997).
- <sup>24</sup>M. Schupkens and G. S. Oehrlein, *Appl. Phys. Lett.* **72**, 1293 (1998).
- <sup>25</sup>J. M. Lane, F. P. Klemens, K. H. A. Bogart, and J. T. C. Lee, *J. Vac. Sci. Technol. A* (submitted).
- <sup>26</sup>M. V. Malyshev, Doctoral thesis, Princeton University, 1999.
- <sup>27</sup>K. H. A. Bogart, J. I. Colonell, V. M. Dannelly, and J. T. C. Lee (unpublished).
- <sup>28</sup>J. P. Chang and H. H. Sawin, *J. Vac. Sci. Technol. A* **15**, 610 (1997).
- <sup>29</sup>H. A. Barker, T. M. Mayer, and W. C. Pearson, *J. Vac. Sci. Technol. B* **1**, 37 (1983).
- <sup>30</sup>P. Kumar, D. S. Bang, J. P. McVittie, and K. C. Sarin, *J. Vac. Sci. Technol. B* **16**, 1123 (1998).
- <sup>31</sup>That portion of the  $\text{SiCl}_4$  etching products that is sputtered during the ion collision cascade, not to be confused with the much slower sputtering of Si by  $\text{Cl}^+$  and  $\text{Cl}_2^+$  in the absence of a flux of neutrals.
- <sup>32</sup>G. S. Hwang and K. P. Giapis, *J. Appl. Phys.* **82**, 572 (1997).
- <sup>33</sup>G. S. Hwang and K. P. Giapis, *J. Vac. Sci. Technol. B* **15**, 70 (1997).
- <sup>34</sup>G. S. Hwang and K. P. Giapis, *J. Appl. Phys.* **85**, 3433 (1997).
- <sup>35</sup>G. Timp et al., *Ultra-Thin Gate Oxides and Ultra-Shallow Junction for High Performance, Sub-100 nm pMOSFETS*, San Francisco, CA, 1998, (BDM Technical Digest (IEEE, Piscataway, NJ, 1998), pp. 10, 41-43).
- <sup>36</sup>K. P. Giapis (private communication).
- <sup>37</sup>S. Wolf, *Silicon Processing for the VLSI Era* (Lattice Press, Sunset Beach, CA 1995), Vol. III.

## BEST AVAILABLE COPY

## Analytical modeling of silicon etch process in high density plasma

Shahram Abdollahi-Alibeik, James P. McVittie, and Krishna C. Saraswat  
Center for Integrated Systems, Stanford University, Stanford, California 94305-4075

Valeriy Sukharev and Philippe Schoenborn  
LSI Logic Corporation, Santa Clara, California 95054

(Received 4 February 1999; accepted 23 April 1999)

Plasma etching of silicon is one of the important etching processes used in modern integrated circuit manufacturing and micro-electro-mechanical systems fabrication. A good understanding of this process leads to better models which are the key to easier and less costly plasma etching process design. The main focus of this paper is on the simulation of the ion reflection from feature sidewalls and the resulting microtrenches. Pure  $\text{Cl}_2$  plasma was used for experiments because of the simple chemistry. SPEEDIE (Stanford etching and deposition profile simulator) was used in this work. Langmuir adsorption model was used for etching kinetics. Self-consistent calculations were done for fluxes using surface coverage dependent sticking probabilities. For ion reflection, it was assumed that the reflected ions come off with a distribution about the specular reflection angle. This distribution is modeled as  $\cos^2\theta$  ( $\theta$  is the deviation from the specular angle) and is important in getting the correct shape for microtrenches in simulations. A three-dimensional (3D) calculation of the reflection flux was done taking into account the 3D angular distribution of the incoming ions. The ion reflection efficiency was deducted from the silicon ion enhanced etching yield versus ion angle of incidence data. The simulation results match the experimental profiles fairly well. © 1999 American Vacuum Society. [S0734-2101(99)04605-9]

## I. INTRODUCTION

The decreasing of feature dimensions in integrated circuit (IC) manufacturing demands more anisotropic and compact etching profiles. Therefore plasma etching, with its ability to produce highly anisotropic etching profiles, is and will be a very important processing step in IC manufacturing. Better understanding of this important process is crucial for further improvement in this field and for developing better processing models.

Plasma etching of silicon is one of the important plasma etching processes used in various IC manufacturing steps. It is used in steps like polysilicon gate etch, formation of DRAM trench capacitors and shallow trench isolation. Various halogen based chemistries are used for this process. The simplest chemistry used is pure  $\text{Cl}_2$ . Since  $\text{Cl}_2$  molecules and  $\text{Cl}$  atoms do not etch silicon at room temperature (except for  $n^+$  doped silicon), this chemistry results in anisotropic etching profiles. In real processes,  $\text{Cl}_2$  is often mixed with other gases such as  $\text{HBr}$  or other halogen containing compounds to increase the control over the etching process and the resulting etching profile.<sup>1-3</sup>

The simplicity of the pure  $\text{Cl}_2$  plasma makes it a good candidate for calibrating and investigating the different phenomena occurring during silicon etching, such as ion reflection and neutral recombination. By understanding these phenomena plasma etching models can be improved. And having good models is the key to easier and less costly plasma etching process design.

Ion reflection is the main focus of this article. The well known connection between microtrenching and ion reflection is first discussed before proceeding to our model for this

reflection and the way reflection fluxes were calculated. Then various aspects of our model are discussed and the agreement between simulation and experimental profiles is shown. The experiments were done in an inductively coupled high density plasma chamber.<sup>4,5</sup>

The simulations presented in this paper were done using SPEEDIE, which is the Stanford etching and deposition profile simulator.<sup>6</sup> This simulator consists of two parts.

- (1) A Monte Carlo simulator for calculating the effect of the plasma sheath on the ions. The output of this part is the ion angular and energy distribution.
- (2) An analytic part which, in a time loop, first calculates the ion and neutral fluxes inside the feature under simulation. From that it calculates the surface etching and deposition rates using appropriate surface kinetics models. These rates are then used for profile evolution. The feature is defined as a series of segments and the surface movement is done by a modified string based method which requires no delooping.

The new models and flux calculations were added to this simulator.

## II. ION REFLECTION AND MICROTRENCHING

For investigating microtrenching phenomenon, a set of etching experiments were done on silicon wafers under different conditions. Trenches with two different openings of 0.4 and 0.8  $\mu\text{m}$  were etched, using 1000-Å-thick  $\text{ITO}$  layer as hard mask. The etchings were done in a Lam TCP9400SE model etch system using pure  $\text{Cl}_2$  gas and a pressure of 10 mTorr. The  $\text{Cl}_2$  gas flow rate was varied between 20 and 100

BEST AVAILABLE COPY

2486

Abdollahi-Ailbelk *et al.*: Analytical modeling of silicon etch process

2486

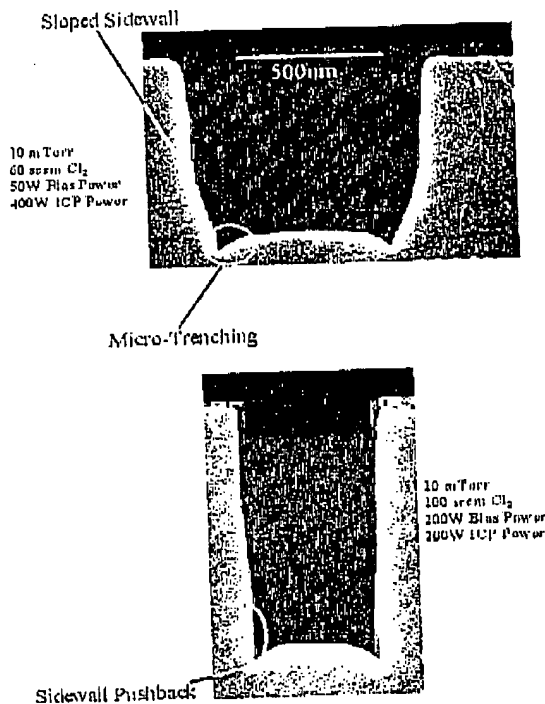


FIG. 1. Silicon trenches etched in an ICP chamber with pure  $\text{Cl}_2$  chemistry. Microtrenching and sidewall pushback effects can be seen in the profiles.

sccm. Three different values for ICP power were used: 200, 400, and 600 W. For bonum power, values of 0, 50, 100, and 200 W were chosen for experiments. The main etching step was done for 120 s. This main etch step was always preceded by a 5 s  $\text{SiO}_2$  breakthrough step.

In Fig. 1 two of these silicon etching profiles can be seen. In both profiles, a local enhancement in the etch rate at the feature corners can be seen, the result of which is called microtrenching. Also in Fig. 1(b), it can be observed that the sidewalls are curved back near the bottom of the trench. This is called sidewall pushback throughout this article.

Since in high density plasmas the neutral-to-ion flux ratio is in the range of 50–500 and since  $\text{Cl}_2$  plasma etching of lightly doped silicon is not spontaneous at the processing temperature used, the etching kinetics is expected to be in the ion limited regime. So a local increase in the etch rate at the feature corners means a local increase in the ion flux here. This fact makes ion reflection a main culprit for microtrench formation.

### III. MODELING

#### A. Etching kinetics

Two kinds of neutral fluxes were considered: etchants ( $F_e$ ) and inhibitors ( $F_i$ ). Etchants were considered to be  $\text{Cl}$

atoms while inhibitors were considered to be  $\text{SiCl}_2$  molecules, which are solid at room temperature.<sup>8,9</sup>

Two different sources can be considered for inhibitors. One source is the plasma gas phase. During the etching process volatile etch products, like  $\text{SiCl}_4$ , will go to the gas phase. If their residence time is long enough (which becomes longer with lower flow rates), they will produce  $\text{SiCl}_2$  molecules. These molecules can come back and stick on the surface of the features.<sup>10</sup>

The other source for inhibitors is the  $\text{SiCl}_2$  molecules locally produced in the feature during etching. The way these products desorb from the surface depends on the actual etching mechanism. If the etching mechanism is ion enhanced chemical etching, the etch products will be thermalized and so they will desorb with a cosine distribution around the normal to the surface. But if etching is done by chemically enhanced sputtering, the etch products desorption distribution will be more like sputtered particles, i.e., they desorb with over cosine distributions around specular angles. It seems that lowering the ion energy or decreasing the ion-to-etchant flux ratio will increase the probability of the ion enhanced chemical etching.<sup>8</sup> Since in high density plasmas, as mentioned before, the neutral-to-ion flux ratio is high, thermalized etching products were assumed in the simulations.

For etching kinetics, Langmuir adsorption model was used, as follows:

$$\sigma \frac{d\theta_e}{dt} = F_e S_e^0 (1 - \theta_e - \theta_i) - \gamma_e F_i \theta_e = 0, \quad (1)$$

$$\sigma \frac{d\theta_i}{dt} = F_i S_i^0 (1 - \theta_e - \theta_i) - \gamma_i F_e \theta_i = 0, \quad (2)$$

$$\text{etch rate} = \frac{Y F_i \theta_e}{\text{density}} \quad (3)$$

in which  $\sigma$  is the site density,  $\theta_e$  and  $\theta_i$  are the surface coverages for etchants and inhibitors, respectively.  $F_e$ ,  $F_i$ , and  $F_d$  are the ion, etchant, and inhibitor fluxes,  $S_e^0$  and  $S_i^0$  are the clean surface sticking probabilities for etchants and inhibitors, and finally  $\gamma_e$  and  $\gamma_i$  are the ion sputtering yields for adsorbed etchants and inhibitors.  $Y$  is the silicon etching yield.

Equalizing the surface coverage derivatives to zero is based on the fact that the surface coverage, at room temperature, reaches its steady state value much faster than the etching rate, i.e., the rate of change in the feature and so in the fluxes.<sup>11</sup>

In etching equations above, only ion enhanced chemical etching was considered. Spontaneous etching was not considered because, as was mentioned before,  $\text{Cl}$  does not etch silicon spontaneously at room temperature (except when  $n^+$  doped). Also physical sputtering yield is much less than ion enhanced chemical etching yield<sup>9,12</sup> and so was ignored.

Simulation parameters were extracted from the data given in the literature.<sup>9,11,13</sup> More specifically,  $S_e^0 = 0.5$  and  $S_i^0 = 0.3$  were used as clean surface sticking probabilities. The etching yields  $\gamma_e$ ,  $\gamma_i$ , and  $Y$  were chosen based on the ion energy. They were assumed to be proportional to  $E_i^{1/2}$

## BEST AVAILABLE COPY

2487 Abdollahi-Allbeik *et al.*: Analytical modeling of silicon etch process

2487

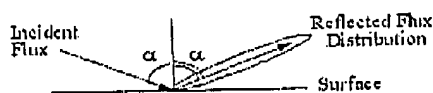


Fig. 2. Reflected ion flux with its distribution about the specular angle.

$-E_i^{1/2}$  ( $E_i$  is the ion energy and  $E_t$  is the threshold energy).<sup>9,12,13</sup> The plasma density and density of different species were calculated using the HPEM/PCMC plasma reactor simulator.<sup>14</sup>

For calculating the neutral fluxes inside the features, surface coverage dependent sticking probabilities were used, in line with Eqs. (1) and (2). This means that the flux on each segment of the feature depends on the surface coverage. But the surface coverage itself depends on the flux the segment receives, according to Eqs. (1) and (2). So the fluxes and surface coverages were solved iteratively to reach to a self-consistent solution.

### B. Ion reflection

It was assumed that ions (which are neutralized before reflection<sup>15,16</sup> and so are actually hot neutrals afterwards, but we refer to them as reflected ions) are reflected at specular angles, with a distribution about the angle of reflection.<sup>18</sup> This point is shown in Fig. 2. Why was perfectly specular reflection not assumed?

Many experiments have been done by researchers on reflection of different ions from different target surfaces.<sup>15-19</sup> Although not that much is done in the field of plasma processing and for the usual materials used in these processes, one thing is common among all reported results and that is the distribution of the reflected ions about the angle of reflection. It will be shown in a later section that this distribution indeed plays an important role in the prediction of the correct shape and depth of the microtrenches.

The distribution about the specular reflection angle was modeled as  $\cos^n \theta$ , in which  $\theta$  is the deviation from the specular reflection angle. Obviously higher  $n$  means tighter distribution and more specular reflection. The value of  $n$ , which is called specularity from now on, depends on different parameters, such as surface material, ion mass, ion energy, and ion angle of incidence.<sup>18</sup> For example, it tends to decrease (less specular reflection) with the increasing of the ion mass (relative to the surface material).

Two other important factors are the ion reflection number efficiency,  $R_n$ , and ion reflection energy efficiency,  $R_e$ . These parameters are also dependent on various factors like ion energy and ion angle of incidence. As was mentioned in the previous section, in etching kinetics formulas, ion flux is always multiplied by a yield factor which itself is roughly proportional to the square root of the ion energy. So the two  $R_n$  and  $R_e$  parameters can be lumped together as one effective  $R_n$  value equal to  $R_n R_e^{1/2}$ .

As mentioned above, not that much information can be found in the literature for the value of reflection parameters for " $\text{Cl}_2$  plasma-Si surface" system and reflection efficiency is not an exception. So this efficiency was estimated by a

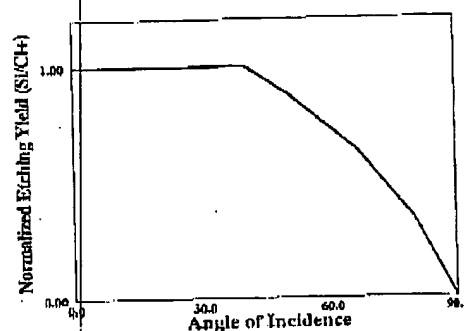


Fig. 3. Silicon ion enhanced etching yield vs ion angle of incidence.

qualitative approach which will be described in the following.

In Fig. 3 the silicon etching yield versus ion angle of incidence is shown.<sup>9,12</sup> As one can see, the etching yield starts to decrease as the angle of incidence (angle to the normal) goes beyond 45°. This decrease in etching yield can be partly due to ion reflection, i.e., ions which hit the surface at large angles to normal will reflect and so their contribution to the etching process will be less. Based on this observation, the curve shown in Fig. 4 was used for  $R_n$ .

One important aspect about this system is that the ion mass ( $\text{Cl}^-$  or  $\text{Cl}_2^+$ ) is actually larger than the target mass (Si). In systems where the ions are lighter than the target,  $R_n$  can be very high even for normal ion incidence.<sup>15-17</sup> But for experiments in which the ion mass is close to the target mass, one sees the same  $R_n$  behavior as here.<sup>18</sup>

A three-dimensional (3D) calculation of the reflection flux was done taking into account the 3D angular distribution of the incoming ions. Furthermore the ion energy distribution was taken into account in etching kinetics calculations.

One simple way for calculating the reflection flux is to keep the 3D incoming ion flux information for each segment of the feature (as was mentioned earlier, the feature is defined as a series of segments) at the time of the direct ion flux calculation and then do the ion reflection flux calculation later. This requires a large amount of memory and time. An-

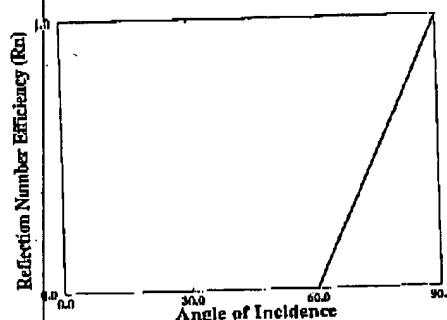


Fig. 4. Ion reflection probability vs ion angle of incidence.

BEST AVAILABLE COPY

2488

Abdollahi-Ailbelk et al.: Analytical modeling of silicon etch process

2488

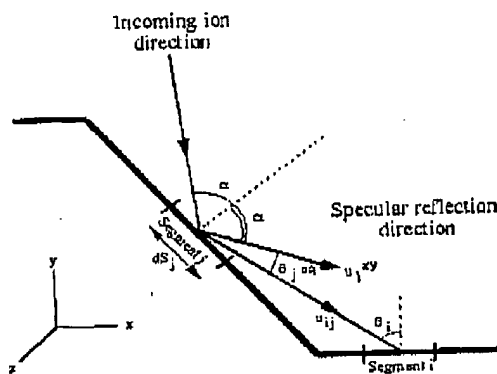


FIG. 5. Incoming and reflected ion fluxes for the sidewall of a trench, projected to  $x$ - $y$  plane.

other option is to do part of the reflection flux calculation during the time of the direct ion flux calculation in such a way that the later calculation of the ion reflection flux will be a two-dimensional (2D) problem rather than a 3D one.

Before describing the method, let us first calculate the reflection flux from one segment to another for different reflection directions. In Fig. 5 a schematic diagram of the incoming and reflection fluxes, projected to the  $x$ - $y$  plane, is shown. It can be shown that the reflection flux which comes off segment  $j$  about the  $u_i$  direction ( $u_i$  is the reflected flux direction if the reflection was perfectly specular) and is received by segment  $i$ , is

$$(\text{flux}_i)_{u_i} = (\text{flux}_i)_{u_i} (\text{flux}_j)_{u_i}^2 \quad (4)$$

$$(\text{flux}_i)_{u_i}^1 = N(n) (\text{fluxref}_j)_{u_i} dS_j \cos^n \theta_{j,u_i} \times a(a^2 + b^2)^{(n-1)/2} \quad (5)$$

$$(\text{flux}_i)_{u_i}^2 = \frac{\cos \theta_i}{r_{ij}} \quad (6)$$

In these equations  $(\text{fluxref}_j)_{u_i}$  is the total ion flux reflected from segment  $j$  about  $u_i$  direction,  $u_i^{xy}$  is the projection of  $u_i$  vector in the  $x$ - $y$  plane,  $u_i^z$  is the component of  $u_i$  in  $z$  direction,  $n$  is the reflection specularity,  $r_{ij}$  is the distance between segments  $i$  and  $j$ , and

$$N(n) = \frac{\Gamma(1/2) \Gamma\left(\frac{n+2}{2}\right)}{\Gamma\left(\frac{n+3}{2}\right)} \frac{n+1}{2\pi} \quad (7)$$

$$a = |u_i^{xy}| \quad (8)$$

$$b = -\frac{u_i^z}{\cos \theta_{j,u_i}} \quad (9)$$

and other parameters are shown in Fig. 5.

J. Vac. Sci. Technol. A, Vol. 17, No. 5, Sep/Oct 1999

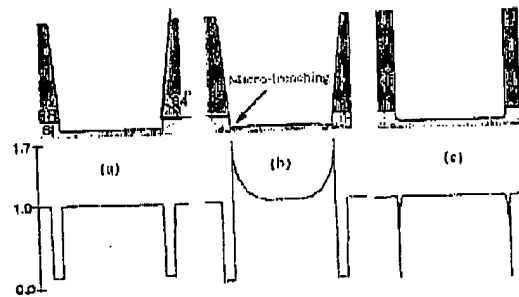


FIG. 6. Three simulation profiles with the normalized ion flux along the feature lengths. (a) No ion reflection. (b) Ion reflection with sloped sidewalls. (c) Ion reflection with steep sidewalls.

One sees that the first part of the reflection flux received by segment  $i$ ,  $(\text{flux}_i)_{u_i}^1$ , only depends on the segment  $j$  information and the direction of the reflected flux. On the other hand the second part,  $(\text{flux}_i)_{u_i}^2$ , only depends on the receiving segment information. So, at the time of the direct ion flux calculation, the first term is calculated for various  $u_{ij}$  directions. Later the reflected flux is calculated by just multiplying the  $(\text{flux}_i)_{u_i}^1$  value of the receiving segment by the  $(\text{flux}_j)_{u_i}^1$  value of the emitting segment.

#### IV. SIMULATION RESULTS AND DISCUSSION

In Fig. 6 simulation profiles together with ion flux along the feature length are shown for three different conditions.

For the profile in Fig. 6(a), the simulation is done with ion reflection turned off. As one sees, there is no increase in the ion flux at the feature corners and so no microtrenching is observed. For Fig. 6(b), the same simulation is shown, but with ion reflection turned on. It can be observed that there is a sharp increase in ion flux at the feature corners. This local increase, as was described earlier, results in an increase of the etch rate at that location and causes microtrenching.

The shape of the feature sidewalls is also very important in the creation and severity of the microtrenches. In Fig. 6(c), a simulation profile is shown for which ion reflection was considered, but simulation was started with steep photoresist sidewalls. No microtrenching is observed. Although the steep sidewalls are still capable of reflecting ions, they do not receive that much ion flux and so substantial enhancement in the ion flux at the feature corners is not expected. This can be seen in the ion flux distribution curve. No increase in ion flux means no microtrenching. In Fig. 7 the effect of sidewall slope is shown in experimental profiles.<sup>20</sup>

Another parameter described earlier was the specularity of the reflected ion flux. To show the importance of this parameter, three simulations (Fig. 8) were done with three different values of  $n$ ,  $n = 1000$ ,  $n = 100$ , and  $n = 50$ . These  $n$  values represent reflected ion angular spreads of about  $2^\circ$ ,  $7^\circ$ ,



(a)



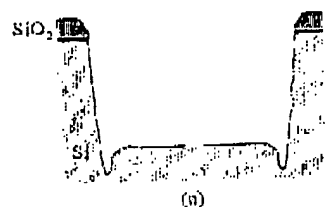
(b)

Fig. 7. Experimental etching profiles for (a) sloped sidewalls and (b) steep sidewalls. The trenches are etched in a reactive ion etching chamber with  $\text{Cl}_2/\text{SiCl}_4/\text{N}_2$  gas mixture (Ref. 20).

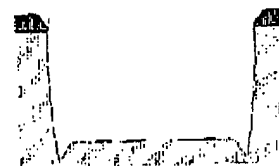
and  $10^\circ$ , respectively. (Here and throughout this article, ion angular spread is defined as the angle at which the ion flux is half its maximum.)

It can be observed in Fig. 8 that the shape of microtrenches are different for these cases. The  $n=1000$  case results in a flatter bottom for microtrenches compared to the  $n=100$  case, which produces sharper microtrenches.  $n=1000$  case also creates deeper microtrenches. In experimental profiles, microtrenches are usually sharp and so perfectly specular ion reflection cannot predict the right shape for microtrenches. By comparing  $n=100$  and  $n=50$  cases [Figs. 8(b) and 8(c)], it can be seen that for less specular ion reflection, micro-trenches are less severe (while they are sharp for both two cases). This may describe, at least partly, the difference observed in microtrenching severity among plasmas with different chemistries (like  $\text{Cl}_2$  and  $\text{HBr}$  plasmas).

In Fig. 9 the simulation profiles are shown for different incoming ion angular spread. For the left-hand side profile the ion angular spread is  $2^\circ$  and for the right-hand side profile this spread is  $5^\circ$ . For both cases the reflected ion flux has



(a)



(b)



(c)

Fig. 8. Simulation profiles for (a)  $2^\circ$ , (b)  $7^\circ$ , and (c)  $10^\circ$  reflected ion angular spread.

a spread of about  $7^\circ$ . The simulations were done with equal ion energy so that the etching profiles could be compared. In reality the cause of change in ion angular spread is usually changing the bottom power and so the dc bias voltage.<sup>21</sup>

As can be seen in Fig. 9, more ion angular spread causes less microtrenching. This has two reasons: for more ion angular spread, more ions hit the sidewalls with angles closer to normal and so the reflection number efficiency will be less. On top of that, these ions will reflect more towards the middle of the trench bottom. Therefore these ions increase the etch rate at the middle instead of the feature corners, as can be seen in the simulation profile.

In Fig. 10 an example of the time evolution of the etching profiles is shown, both from experiments and simulations. It can be seen that as etching proceeds, more sidewall becomes

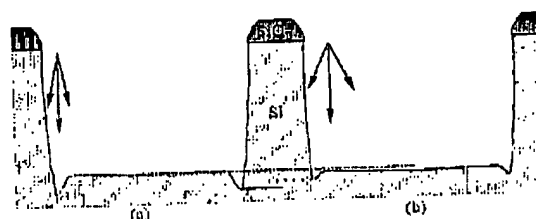


Fig. 9. Simulation profiles for (a)  $2^\circ$  and (b)  $5^\circ$  incoming ion angular spread (with the same reflected ion angular spread of  $7^\circ$ ).

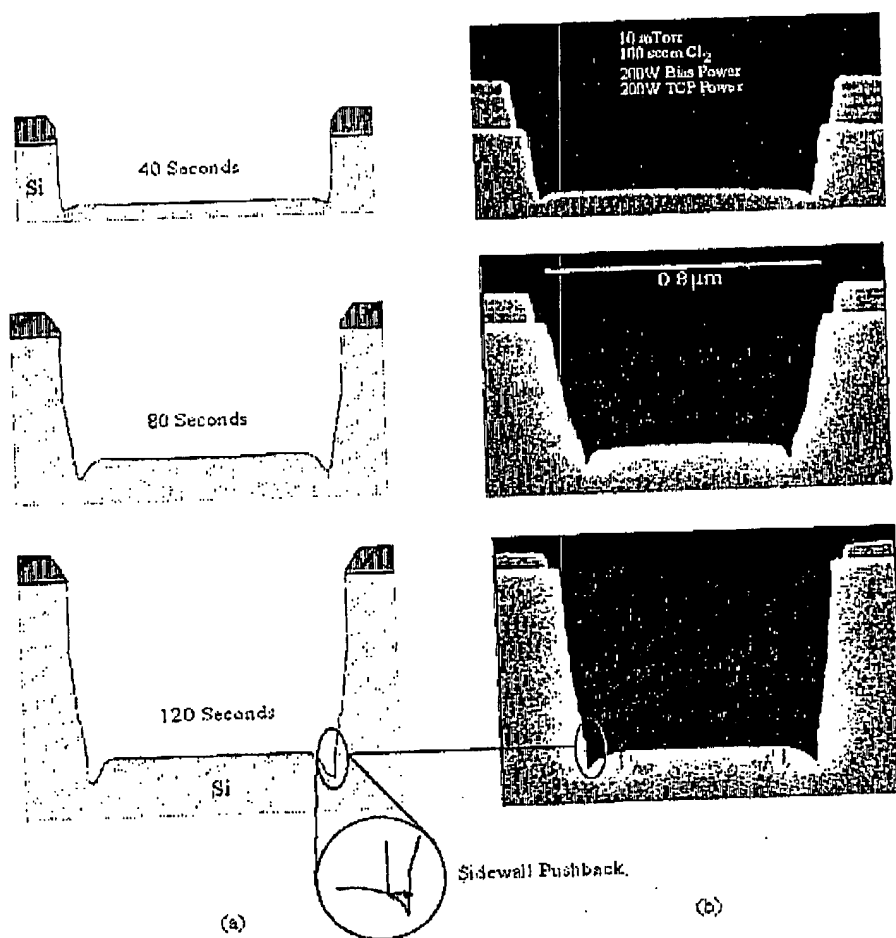


FIG. 10. Change in microtrenches with time: (a) simulation; (b) experiment. The mechanism for sidewall pushback is also shown at the bottom.

available for ion reflection, hence microtrenches become deeper and wider with time. For the  $t = 120$  s profile, the phenomenon called sidewall pushback is revisited. As shown in Fig. 10 inset, this happens because of ion reflection from the other side of the microtrench. These ions hit the sidewall and cause an increase in the sidewall etch rate. This reflection becomes more important when the microtrenches become wider and deeper, as happens through the time. This phenomenon is also captured in the simulation, as can be seen in Fig. 10.

## V. CONCLUSION

Microtrenching and hence ion reflection from feature sidewalls are important factors in shaping the etching profiles and are very important to investigate. It was shown that ion reflection alone cannot result in microtrenching and that feature sidewall slope is also an important factor in the formation of the microtrenches. Also it was shown that the in-

coming ion angular distribution as well as the angular distribution of the reflected ions play an important role in the shape and depth of the microtrenches. The simulations matched the experimental profiles fairly well.

The strength of our simulation method is that it is analytic as opposed to Monte Carlo methods used in many other etching simulation programs. The simulation times for the simulation profiles shown in this article were all less than 90 min on an IBM RS6000 computer.

## ACKNOWLEDGMENTS

The authors would like to thank the members of the SPEEDIE group at Stanford University for their useful suggestions on different aspects of this project. They would also like to acknowledge the Semiconductor Research Corporation and DARPA for their financial support.

BEST AVAILABLE COPY

2491

Abdollahi-Alibolk et al.: Analytical modeling of silicon etch process

2491

- <sup>1</sup>A. Grill, *Cold Plasma in Materials Fabrication: Fundamentals to Applications* (IEEE, New York, 1994), pp. 231-234.
- <sup>2</sup>C. S. Oehrlein, in *Handbook of Plasma Processing Technology*, edited by S. M. Rossnagel, J. J. Cuomo, and W. D. Westwood (Noyes, Park Ridge, NJ, 1990), pp. 200-211.
- <sup>3</sup>D. L. Flamm, V. M. Donnelly, and D. E. Ibbotson, in *VLSI Electronics: Microstructure Science*, edited by N. G. Einspruch, and D. M. Brown (Academic, Orlando, FL, 1984), Vol. 8, pp. 190-252.
- <sup>4</sup>R. Patrick, P. Schoenbarn, F. Bose, and H. Toda, *J. Vac. Sci. Technol. A* **11**, 1296 (1993).
- <sup>5</sup>J. B. Carter et al., *J. Vac. Sci. Technol. A* **11**, 1301 (1993).
- <sup>6</sup>J. P. McVittie et al., *SPEEDIE 3.0 Manual* (Stanford University, 1996).
- <sup>7</sup>C. M. Anderson, G. S. Hwang, M. J. Gordon, and K. P. Giapis, *Proc. Electrochem. Soc.* **12**, 357 (1996).
- <sup>8</sup>H. F. Winters and J. W. Coburn, *Surf. Sci. Rep.* **14**, 161 (1992).
- <sup>9</sup>J. P. Chang et al., *J. Vac. Sci. Technol. A* **16**, 217 (1998).
- <sup>10</sup>C. Lee, D. B. Graves, and M. A. Lieberman, *Plasma Chem. Plasma Processing* **16**, 99 (1996).
- <sup>11</sup>A. D. Bailey III, M. C. M. van de Sanden, J. A. Gregus, and R. A. Gonscho, *J. Vac. Sci. Technol. B* **13**, 92 (1995).
- <sup>12</sup>J. P. Chang and H. H. Sawin, *J. Vac. Sci. Technol. A* **15**, 610 (1997).
- <sup>13</sup>C. C. Cheng, K. V. Ginn, V. M. Donnelly, and I. P. Herman, *J. Vac. Sci. Technol. A* **12**, 2630 (1994).
- <sup>14</sup>P. L. G. Ventzek, M. Grapperhaus, and M. J. Kushner, *J. Vac. Sci. Technol. B* **12**, 3118 (1994).
- <sup>15</sup>J. W. Cuthbertson, R. W. Motley, and W. D. Langer, *Rev. Sci. Instrum.* **63**, 5279 (1992).
- <sup>16</sup>J. W. Cuthbertson, Ph.D. thesis, Princeton University, 1991.
- <sup>17</sup>J. W. Cuthbertson, W. D. Langer, and R. W. Motley, *J. Nucl. Mater.* **196-198**, 113 (1992).
- <sup>18</sup>W. Reikstein and J. P. Hiersack, *Z. Phys. B: Condensed Matter* **63**, 109 (1986).
- <sup>19</sup>D. N. Ruzic, in *Handbook of Plasma Processing Technology*, edited by S. M. Rossnagel, J. J. Cuomo, and W. D. Westwood (Noyes, Park Ridge, NJ, 1990), pp. 76-80.
- <sup>20</sup>N. J. Mulaf et al., *J. Vac. Sci. Technol. B* **7**, 1497 (1989).
- <sup>21</sup>J. Zheng, R. P. Brinkmann, and J. P. McVittie, *J. Vac. Sci. Technol. A* **13**, 859 (1995).

## BEST AVAILABLE COPY

## Microtrenching resulting from specular reflection during chlorine etching of silicon

Robert J. Hoekstra<sup>a)</sup> and Mark J. Kushner<sup>b)</sup>  
*Department of Electrical and Computer Engineering, University of Illinois, 1406 W. Green St.,  
 Urbana, Illinois 61801*

Valeriy Sukharev and Phillippe Schoenborn  
*LSI Logic Corporation, 3115 Alfred St., Santa Clara, California 95054*

(Received 9 February 1998; accepted 10 April 1998)

In an effort to increase throughput, the microelectronics fabrication industry has transitioned to high plasma density etching reactors using large source ( $>800$  W) and moderate substrate bias ( $>100$  W) powers in which the ion to neutral radical flux is large compared to reactive-ion-etching systems. These conditions can lead to microtrenching where etch rates are largest at the base of the sidewalls. Microtrenching has been attributed to specular reflection of high energy particles, usually ions, at grazing angles on the sidewalls of the mask and trench. These reflections produce a "focusing" of flux to the corners of the trench which results in locally enhanced etching. In this letter, integrated plasma equipment and Monte Carlo feature profile models have been used to examine the processes and conditions which produce focused fluxes and microtrenching, including the degree of specular reflection and sidewall slope of the mask. Quantitative comparisons are made to experimental measurements of etch profiles. © 1998 American Vacuum Society.  
 [S0734-211X(98)00804-X]

As the feature sizes of microelectronics devices decrease to sub- $0.5\ \mu\text{m}$  dimensions, the semiconductor fabrication industry is increasingly employing dry etching techniques using high plasma density reactors such as inductively coupled plasma (ICP) systems.<sup>1</sup> These tools differ from conventional reactive-ion-etching (RIE) reactors in that the ratio of the ion flux to the reactive neutral flux to the substrate is larger. Microtrenching is one possible consequence of these conditions. Microtrenching refers to profiles for which the etch rate is larger near the corners of a trench compared to the center of the trench. The etch profile across the floor of the trench is therefore either convex or has vertical slots at the base of the sidewalls. Microtrenching is believed to be produced by the impact of high energy particles (mostly ions) at grazing angles ( $>80^\circ$ ) on the sidewalls followed by specular reflection where the particles retain a large fraction of their energy and directionality. These conditions lead to "focusing" of the high energy particles at the base of the sidewalls of the feature, resulting in higher etch rates at those locations. Microtrenching can lead to large differences in etch depth across the bottom of features and the possibility of "punchthrough" on etch stops or other thin layers such as gate oxide. Microtrenching was first discussed by Nguyen *et al.*,<sup>2</sup> and the proposal that specular reflection is a major contributing cause was first made by Dalton *et al.*<sup>3</sup>

As plasma equipment models and profile simulators have matured, the ability to self-consistently predict the consequences of plasma-surface interactions on etch profiles has also significantly improved.<sup>4-7</sup> In this regard, in this letter we present results from integrated plasma equipment and profile

models to investigate the consequences of specular reflection by high energy grazing-angle ions and neutrals on profile evolution during chlorine plasma etching of Si. The plasma simulator we used in this study is the hybrid plasma equipment model (HPEM) and the profile simulator is the Monte Carlo feature profile model (MCFPM). The models, and their method of integration, are described in Refs. 4 and 8. In the MCFPM, the trench is resolved in two dimensions using a rectilinear numerical mesh having  $500 \times 500$  cells for a  $1\ \mu\text{m} \times 1\ \mu\text{m}$  region. Computational particles are directed towards the surface representing the energy and angularly resolved ion and neutral fluxes produced by the HPEM. Monte Carlo techniques are applied to changed the identity of a mesh cell to represent, for example, adsorption, passivation, and etching processes. The reaction mechanism we used is based on successive chlorination of Si by neutral Cl atoms followed by ion stimulated desorption of  $\text{SiCl}_n$ .<sup>4</sup>

The MCFPM differs from that previously described in the method of treating ion (or high energy neutral) reflections from surfaces. Due to the statistically rough surface inherent to Monte Carlo based simulators, it is necessary to locally smooth the surface at the site of impact to eliminate unrealistic high angle scattering from sharp boundaries of the numerical mesh between the surface and plasma. This smoothing was accomplished by sampling the actual plasma-surface boundary 10–20 cells on either side of the point of impact and making a least-squares fit to the surface. The incident particle then collides and reflects from the smoothed surface.

All experimental and model results discussed in this article are for an inductively coupled LAM 9400SC plasma etching reactor.<sup>9</sup> The reactor operating parameters are: 600 W inductively coupled power, 100 W substrate bias at 13.56 MHz, and 10 mTorr of  $\text{Cl}_2$  at a flow rate of 60 sccm. The

<sup>a)</sup>Electronic mail: stretch@uipehn.ecu.uiuc.edu  
<sup>b)</sup>Electronic mail: mjk@uiuc.edu

BEST AVAILABLE COPY

2103

Hookstra *et al.*: Microtrenching resulting from specular reflection

2103

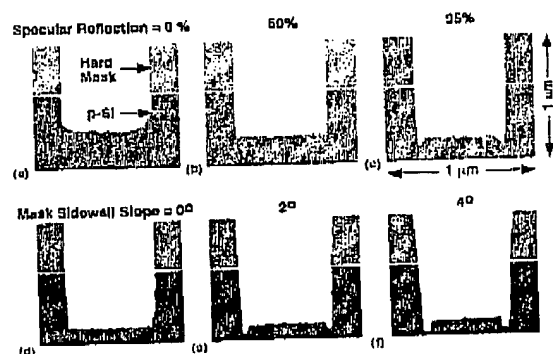


FIG. 1. Etch profiles for chlorine etching of silicon for (a) 0%, (b) 50%, and (c) 95% specular reflection and for outward slope of the mask sidewalls of (d) 0°, (e) 2°, and (f) 4°.

system we are addressing is etching of crystalline Si using a hard mask of  $\text{SiO}_2$ . The angular dependence of the etch yield of chlorine atomic ions on silicon we used in the MCFPM is that measured by Chang and Sawin.<sup>10</sup> We specified that ions retain as much as 99% of their energy when reflecting at grazing angles ( $>80^\circ$ ) based on results from molecular dynamics simulations by Helmer and Graves.<sup>11</sup> We ignored the effects of surface charging on ion trajectories in the trench due to the moderately high conductivity of the substrate, though charging in the trench is an important process in producing notching.<sup>12</sup>

To demonstrate the dependence of microtrenching on the degree of specular reflection (SR), the fraction of grazing ions allowed to retain their energy was varied from 0% to 95%. The resulting profiles, shown in Figs. 1(a)–1(c) for 0.6  $\mu\text{m}$  wide trenches, reveal significant changes in the morphology of the bottom of the trench. As the fraction of SR is increased, the corners of the trench evolve from being rounded at 0% SR, to being sharp and square at 50%, and finally to having microtrenches at the base of the sidewalls at 95% SR. The onset of microtrenching is a direct result of ion reflection from the sidewalls leading to "focusing" or enhancement of the particle flux at the base of the sidewall. The increased particle flux produces a higher etch rate which, if sufficiently focused, generates microtrenching, generally at  $\text{SR} > 90\%$ .

The slope of the sidewall of the mask can also play an important role in the initial development of microtrenching. A finite slope of the mask increases the solid angle of the ion flux from the plasma that can reflect from its sidewalls. Since the angular spreads of the ion flux for the conditions of interest are typically  $<4^\circ$ – $5^\circ$ , a small variation in the slope of the mask sidewall accesses a significantly larger fraction of the ion flux. For example, the etch profiles shown in Figs. 1(d)–1(f) were obtained by varying the slope of the mask sidewalls from  $0^\circ$  to  $4^\circ$ . As the slope is increased the microtrenching becomes more pronounced and broader. Note that as the depth of the trench increases the relative area of

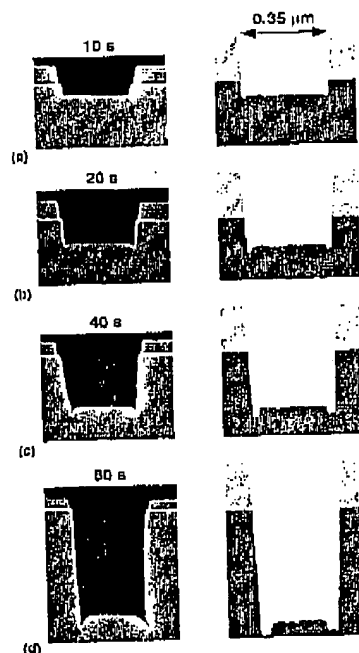


FIG. 2. Comparison of experimental etch profiles (left-hand side) and results from the model (right-hand side) for etch times of (a) 10, (b) 20, (c) 40, and (d) 80 s.

the mask sidewall decreases compared to the exposed sidewall of the trench. Therefore the influence of the slope of the mask on microtrenching is less pronounced for deeper trenches. However, since the solid angle of the ion flux accessible by the sidewalls of the mask is always larger than that for the trench, its slope is always an important consideration.

The evolution of microtrenching is shown in Fig. 2 where predictions from the simulation are compared to experimental results for 0.35  $\mu\text{m}$  wide trenches at different times during the etch. A 0.2  $\mu\text{m}$  thick hard mask was used in the model, while a 0.1  $\mu\text{m}$  hard mask was used experimentally which etched at a rate approximately 5% that of the silicon. The predicted and experimental profiles show the same trends. As the trench deepens, the depth and width of the microtrenches increases as more sidewall area is available to reflect and focus ions. The model shows a more severe broadening of the microtrenches than found in the experiments which may be a consequence of the discreteness of the numerical mesh.

The angular dependence of sputtering yield is typically depressed at normal incidence with a maximum near  $60^\circ$  as recently demonstrated by molecular dynamics simulations by Hanson *et al.*<sup>13</sup> for the sputter yield of  $\text{Cl}^+$  on Si. Experiments by Chang and Sawin,<sup>10</sup> however, show a broad maximum in the etch yield of  $\text{Cl}^+$  on Si from  $0^\circ$  to  $40^\circ$  with a gradual decrease approaching  $90^\circ$ . These results indicate that

BEST AVAILABLE COPY

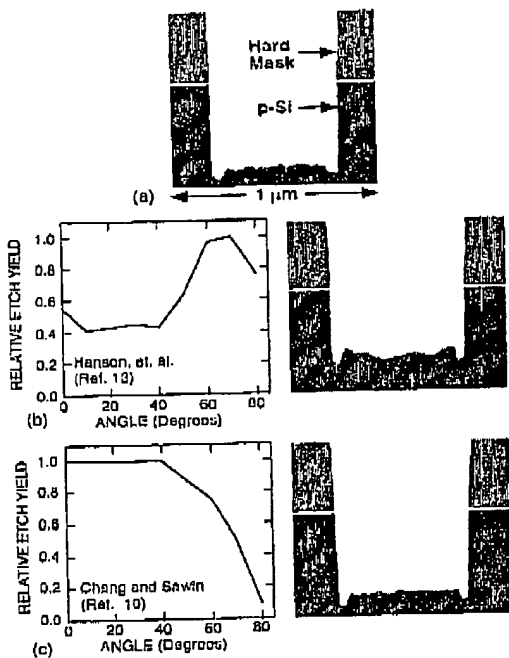


FIG. 3. Etch profiles for different models of the angular dependence of etch yield. (a) Uniform angular dependence, (b) angular dependence as given by Hanson *et al.* (Ref. 13), shown at left for 100 eV ions, (c) angular dependence as given by Chang and Sawin (Ref. 10), shown at left for 35 eV ions.

the mechanism for ion enhanced etching may differ from simple sputtering. The precise forms of these etch yields do have an influence on microtrenching. These trends are shown in Fig. 3 where profiles are plotted for the same etch times while using different angular dependencies for the etch yield. The slope of the mask sidewall is 2°. The profile in Fig. 3(a), the base case, was obtained with no angular dependence of the etch yield. The sidewalls of the trench have a shallow angle and the microtrench is broad due to there being a broad angular flux of reflected ions. The profile in Fig. 3(b) was obtained using the angular dependence of Hanson *et al.* The etch rate is smaller than for the base case since the relative etch yield at near normal incidence is lower. The sidewalls are nearly vertical due to the larger etch yield at grazing angles. There is also structure on the floor of the trench resulting from the extrema in the etch yield and energy loss of

ions reflecting from the walls. The profile generated using the etch yields from Chang and Sawin [Fig. 3(c)], has narrower microtrenches than the base case, due to there being fewer losses of grazing incidence ions on the sidewalls. The sidewall slope is larger than for the yields of Hanson *et al.* due to the decrease in etch yield at grazing angles. The total etch rate is commensurate with the base case due to the larger yield at normal angles.

In conclusion, a Monte Carlo feature profile model has been used to investigate the effects of specular reflection of grazing-angle ions on the profile evolution and microtrenching in chlorine plasma etching of silicon. We found that the SR of ions from the sidewalls must exceed 90% at grazing incidence ( $>80^\circ$ ) to reproduce experimentally observed microtrenching. The slope of the sidewall of the mask also has an important influence on microtrenching. Sidewall slopes of  $2^\circ$ – $4^\circ$ , commensurate with the angular spread of the incoming ion flux, increases microtrenching by accessing a larger solid angle of the ions. The angular dependence of the etch yield influences microtrenching as well. Low yields at high angles of incidence allow more ions to retain a larger fraction of their energy after reflection from the sidewalls, thereby producing a narrower microtrench. Microtrenching increases with increasing etch depth due to the larger sidewall area available for ion reflection.

This work was supported by the Semiconductor Research Corporation, National Science Foundation (ECS 94-04133, CTS 94-12565), and the University of Wisconsin ERC for Plasma Aided Manufacturing.

- <sup>1</sup>J. H. Keller, *Plasma Sources Sci. Technol.* **5**, 166 (1996).
- <sup>2</sup>S. V. Nguyen, D. Dobuzinsky, S. Stiller, and G. Christman, *J. Electrochem. Soc.* **138**, 1112 (1991).
- <sup>3</sup>T. J. Dolan, J. C. Arnold, H. H. Sawin, S. Swan, and D. Cortiss, *J. Electrochem. Soc.* **140**, 2395 (1993).
- <sup>4</sup>R. J. Hoekstra, M. J. Grapperhaus, and M. J. Kushner, *J. Vac. Sci. Technol.* **A 15**, 1913 (1997).
- <sup>5</sup>V. Singh, F. S. G. Shafiq, and J. P. McVittie, *J. Vac. Sci. Technol.* **B 12**, 2952 (1994).
- <sup>6</sup>B. Abraham-Shrauner and W. Chen, *J. Vac. Sci. Technol.* **B 14**, 3492 (1997).
- <sup>7</sup>N. Hamaguchi and S. M. Rossnagel, *J. Vac. Sci. Technol.* **B 13**, 183 (1995).
- <sup>8</sup>M. J. Grapperhaus and M. J. Kushner, *J. Appl. Phys.* **81**, 569 (1997).
- <sup>9</sup>LAM Research Corp., Fremont, CA; URL <http://www.lamrc.com>
- <sup>10</sup>J. Chang and H. H. Sawin, *J. Vac. Sci. Technol.* **A 15**, 610 (1997).
- <sup>11</sup>B. A. Helmer and D. D. Graves, presented at the 44th Annual Symposium of the American Vacuum Society, San Jose, CA, October 1997, paper 15S-THA10.
- <sup>12</sup>G. S. Hwang and K. P. Giapis, *J. Vac. Sci. Technol.* **B 15**, 70 (1997).
- <sup>13</sup>D. E. Hanson, A. F. Voter, and J. D. Kress, *J. Appl. Phys.* **82**, 3552 (1997).

## BEST AVAILABLE COPY

## Feature evolution during plasma etching. II. Polycrystalline silicon etching

J. M. Lane, F. P. Klemens, K. H. A. Bogart,<sup>1)</sup> M. V. Malyshev, and J. T. C. Lee  
*Bell Laboratories, Lucent Technologies, Murray Hill, New Jersey 07974*

(Received 12 April 1999; accepted 10 September 1999)

The effect of source power, bias power, chamber pressure, flow rate, and feed gas composition on profile evolution during polycrystalline silicon etching with an oxide hardmask has been studied in a transformer-coupled plasma system. The large resultant data set provides a comprehensive look at feature evolution as plasma parameters are varied. This data set is valuable for evaluating the importance of several proposed mechanisms for feature evolution and for validating computational models. Microtrench formation was found to be a strong function of the plasma condition. A correlation between sidewall shape and microtrench development was observed. Profile development was found to be highly sensitive to feed gas composition. Results are consistent with a previous study on the etching of crystalline silicon under identical plasma conditions. © 2000 American Vacuum Society. [S0734-2101(00)00901-5]

## I. INTRODUCTION

A more detailed understanding of plasma etching processes is vital as the semiconductor industry continues to demand smaller feature widths. Specifically, an understanding of the anomalies that develop within trench features—such as microtrenches, bowed sidewalls, and undercut hardmasks—will be necessary to design future generation etching tools and processes. This study provides an experimental data set for viewing the feature evolution process as plasma parameters are varied. To preface the discussion of results, a brief overview is provided here of several common feature profile anomalies and the mechanisms proposed to account for them. Aspect ratio dependent etching, microtrench formation, bowed sidewalls, and hardmask undercut are discussed.

Aspect ratio dependent etching, where high aspect ratio features etch slower than their low aspect ratio counterparts, is often attributed to geometric shadowing of neutral species.<sup>1–5</sup> Neutrals have an isotropic distribution at the wafer surface. The bottoms of higher aspect ratio features have less visibility to the plasma, therefore, the flux of neutrals is decreased and leads to a lower etching rate.

Microtrenches, sometimes called arches or dovetails, are frequently observed at feature bottoms.<sup>4,6–8</sup> This phenomenon is often attributed to off-angle ions scattering at grazing angles from feature sidewalls. Scattered ions can become “focused,” creating a localized area with an accelerated etching rate. A diagram of ion reflection is shown in Fig. 1(a). Additionally, ion trajectories may be skewed in local electric field created by a negatively charged insulating mask layer.<sup>5,9–12</sup> This mechanism would provide another source of off-angle ions within the trench to impact upon and be focused by feature sidewalls, as shown in Fig. 1(b). Ions arrive at the wafer with a narrow angular distribution, after acceleration across the plasma sheath. Conversely, the plasma sheath decelerates electrons, resulting in a more isotropic distribution. As more electrons than ions impinge on an in-

insulating sidewall, a negative charge can accumulate. This creates an electric field that can divert the path of incoming ions toward the sides of the feature.

Angled or bowed sidewalls can develop and focusing of scattered ions could be sensitive to feature sidewall curvature. The ion trajectories within the trench could be responsible for the sidewall shape.<sup>6,7</sup> Ions that impact the sidewalls at grazing angles will likely scatter specularly, retaining nearly all of their initial energy, while ions that impact at greater angles could etch the sidewalls.

Another mechanism that may affect feature profiles is deposition or redeposition within a feature.<sup>13–15</sup> As etching progresses, etch products could redeposit on the wafer after production in the trench or fragmentation in the plasma. This deposition could build in the feature, accumulating on the sidewalls and causing a taper.<sup>4</sup>

Several computational models have been developed to simulate profile development and validate the mechanisms described earlier.<sup>3,6,8,16–18</sup> These simulators are typically tested against a set of experimental profiles. The simulators have advanced to the point that they are self-consistent with the experimental profiles they were designed to predict. However, in order to simulate all proposed mechanisms and their relative importance at various plasma conditions, it is necessary to have an experimental set of data that record the evolution of a simple feature while plasma conditions are

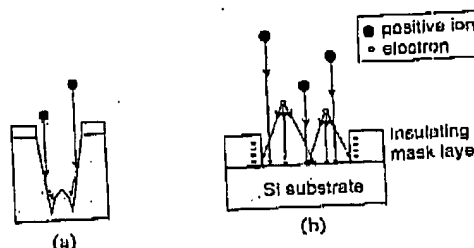


Fig. 1. Diagrams for mechanisms of (a) ion steering and (b) charging of an insulating mask layer.

<sup>1)</sup>Electronic mail: kbogart@lucent.com

## BEST AVAILABLE COPY

189

Lane et al.: Feature evolution during plasma etching

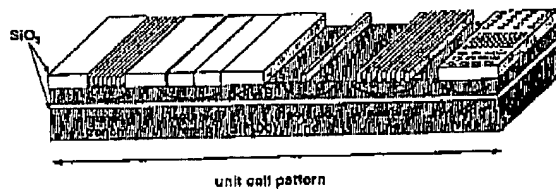


FIG. 2. Illustration of the film stack and the unit cell pattern used during experimental etching.

varied. Some studies have been conducted to this end.<sup>4,5,19</sup> However, few are simplistic enough, utilizing a single-gas chemistry or a simple feature, to truly isolate the mechanisms involved in feature profile evolution.

Recently, a comprehensive investigation into feature evolution during high-density chlorine ( $\text{Cl}_2$ ) plasma etching in crystalline silicon [ $\text{Si}(100)$ ] was conducted.<sup>20</sup> A full factorial set of plasma conditions—varying bias power, source power, and pressure—was investigated. One condition was duplicated in a  $\text{HBr}$  plasma. The degree of microtrench formation decreased as pressure was lowered from 10 to 2 mTorr, increasing bias power, or substituting  $\text{Cl}_2$  feed gas with  $\text{HBr}$ . Etching rate was found to be independent of the feature aspect ratio.

The complementary study presented here expands that work by investigating  $\text{Cl}_2$  plasma etching of polycrystalline silicon (poly-Si) and broadens the set of plasma conditions in order to provide a more detailed description of the effect of plasma parameters on feature profile and to observe feature evolution in a common transistor gate stack material. A discussion is conducted of the qualitative agreement between these experimental results and the proposed mechanisms outlined earlier.

## II. EXPERIMENT

### A. Wafer preparation and etching system

$\text{Si}(100)$  wafers (150 mm) with thermally grown  $\text{SiO}_2$  (1000 Å thick) were used as substrates. Poly-Si films, 1.0  $\mu\text{m}$  thick, were deposited and then annealed at 500°C to achieve a polycrystalline rather than amorphous structure.  $\text{SiO}_2$  mask material (5000 Å thick) was deposited by plasma enhanced chemical vapor deposition and patterned in  $\text{CHF}_3/\text{SF}_6$  plasmas using photoresist masks. The resulting patterned oxide was used as a hardmask during the etching

189

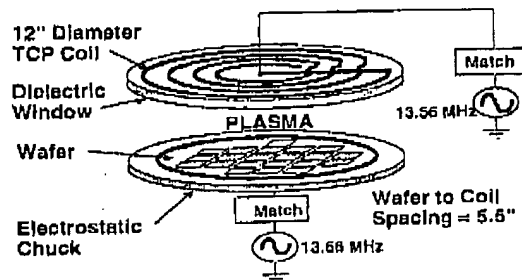


FIG. 3. Schematic of Lam TCP 9400Si<sup>TM</sup> plasma etching system.

of the underlying poly-Si. The test pattern, along with the material stack, is shown in Fig. 2. The pattern consisted of isolated lines, isolated trenches, nested lines, nested trenches, and windows. Feature length scales of nominally 0.6, 0.35, and 0.30  $\mu\text{m}$  were examined.

Etching of the poly-Si films was performed on a Lam TCP 9400Si<sup>TM</sup> high-density plasma etching system.<sup>21</sup> The system is shown schematically in Fig. 3. The plasma was generated by a 305 mm diameter flat coil antenna powered at 13.56 MHz. The substrate was biased by an independently controlled 13.68 MHz power supply. Wafers were electrostatically clamped to a substrate holder and He backside cooling was used to maintain the wafer temperature at 60°C.

### B. Experimental conditions

The experimental variables studied were rf source power, rf bias power, chamber pressure, feed gas composition and flow rate. Eight  $\text{Cl}_2$  plasma conditions and one  $\text{HBr}$  plasma condition, identical to those in the complementary study of  $\text{Si}(100)$  etching, were investigated (Table I, conditions 1–9). The parameter space was extended to include six more plasma conditions (Table I, conditions 10–15). Features 0.5 and 0.9  $\mu\text{m}$  deep were etched under these 15 plasma conditions to investigate the effect of aspect ratio.

A schematic of an etched trench is shown in Fig. 4. For aspect ratio calculations, measurements were taken of (1) the feature width, (2)  $d_{\text{min}}$ , the distance from the top of the hardmask to the center of the trench, and (3)  $d_{\text{micro}}$ , the distance from the top of the hardmask to the bottom of the microtrench. For etching rates,  $d_{\text{min}}$  and  $d_{\text{micro}}$  were measured from the top of the poly-Si. From these measurements,

TABLE I. Listing of experimental etching conditions used in the present study.

Condition	1	2	3	4	5	6	7	8	9	10	11	12	13	14	15
rf source power (W)	250	500	250	500	250	500	250	500	500	250	250	250	750	500	500
rf bias power (W)	150	150	250	250	150	150	250	250	150	350	150	150	150	150	150
Pressure (mTorr)	2	2	2	2	10	10	10	10	10	10	25	50	10	10	10
Chemistry	$\text{Cl}_2$	$\text{Cl}_2$	$\text{Cl}_2$	$\text{Cl}_2$	$\text{Cl}_2$	$\text{Cl}_2$	$\text{Cl}_2$	$\text{Cl}_2$	$\text{HBr}$	$\text{Cl}_2$	$\text{Cl}_2$	$\text{Cl}_2$	$\text{Cl}_2$	$\text{HCl}$	$\text{Cl}_2$
Flow (sccm)	80	80	80	80	80	80	80	80	80	80	80	80	80	80	40
Depth ( $\times 1000$ Å)	5	5	5	5	5	5	5	5	5	5	5	5	5	5	-
	9	9	9	9	9	9	9	9	9	9	9	9	9	9	9

## BEST AVAILABLE COPY

190

Lane et al.: Feature evolution during plasma etching

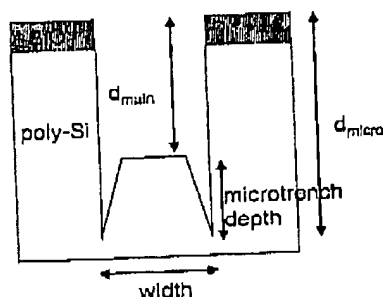


Fig. 4. Illustration of measurements made of etched trench features.

two etching rates ( $d_{\text{main}}/\text{time}$  and  $d_{\text{micro}}/\text{time}$ ) and two corresponding aspect ratios were calculated. The significance of these two measurements will be discussed in Sec. III A. The severity of the microtrench was quantified by expressing the microtrench depth as a percentage of  $d_{\text{main}}$ .

### III. RESULTS AND DISCUSSION

The collection of scanning electron microscopy (SEM) data is displayed and discussed later with an eye toward possible mechanisms. It is important to note that any profile skew observed is not genuine, but rather an artifact of sample drift during the SEM process. An example of a nested trench, isolated trench, and isolated line after the hardmask etch, with photoresist still intact, is shown in Fig. 5. The hardmask sidewall forms an angle of  $82^\circ$  with the wafer surface. This angle is constant across feature type. Several profile evolution models show that trench development is sensitive to this angle.<sup>4,8</sup> In this study, the hardmask angle remained relatively constant across feature type and size, and the effect of changing this angle was not investigated.

#### A. Etching rates and aspect ratio dependent etching (ARDE)

In the first eight chlorine plasma conditions, corresponding to the conditions previously studied using Si(100),<sup>20</sup> two

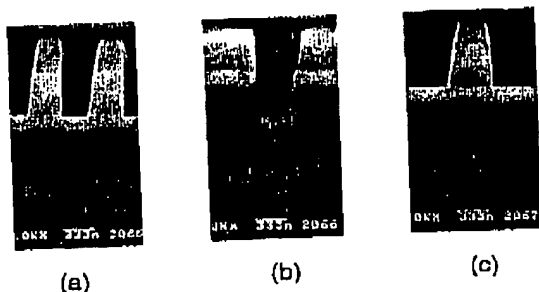


Fig. 5. Cross sections of nominally  $0.35 \mu\text{m}$  (a) nested trench, (b) isolated trench, and (c) isolated line patterned hardmask profiles before poly-Si etching with photoresist still intact.

J. Vac. Sci. Technol. A, Vol. 18, No. 1, Jan/Feb 2000

2 mTorr

(a)

(b)

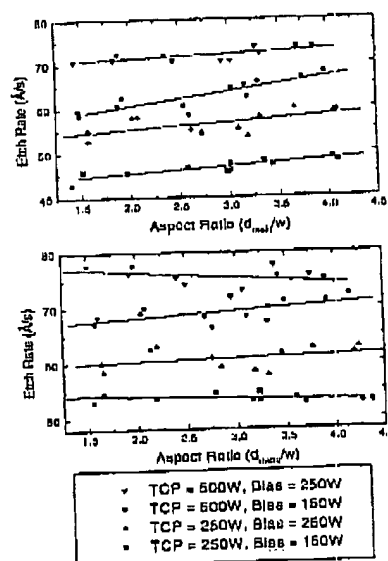


Fig. 6. Etch rate vs aspect ratio at 2 mTorr calculated using (a)  $d_{\text{main}}$  and (b)  $d_{\text{micro}}$ .

different aspect ratios were defined as the ratio of the depth of a feature to its width:  $d_{\text{main}}/w$  and  $d_{\text{micro}}/w$  (Fig. 3), and were calculated for each trench.

The etching rate dependence on  $d_{\text{main}}/w$  [Fig. 6(a)] and  $d_{\text{micro}}/w$  [Fig. 6(b)] aspect ratios for nested features at 2 mTorr under four different  $\text{Cl}_2$  plasma conditions are plotted in Fig. 6. The analogous plots at 10 mTorr are shown in Fig. 7. The data contain scatter, and the lines drawn through the points are not a linear fit, but are meant to guide the eye. As expected, etching rates increased with increasing source or bias powers due to increased ion flux and increased ion energy (etching yield), respectively. Significant ARDE was not observed either at 2 or at 10 mTorr. This suggests that the geometric shadowing of neutrals, either at the feature center or side, does not play a significant role in etching rate under these plasma conditions.

#### B. Nested trenches

All features—nested trenches, nested lines, isolated lines, isolated trenches, and windows—exhibited similar qualitative profile development. Development of the nested features will be discussed in detail, followed by an examination of how the other features varied slightly from the nested trenches. A schematic of trench bottom and sidewall development, with accompanying definitions, is shown in Fig. 8. Feature profiles resulting from the full-factorial chlorine plasma experiment (Table 1, conditions 1–8) are shown in Figs. 9–12. The horizontal axis represents source power. Profiles etched with 250 W source power are shown on the left, and those etched with 500 W source power are on the

## BEST AVAILABLE COPY

191

Lane et al.: Feature evolution during plasma etching

191

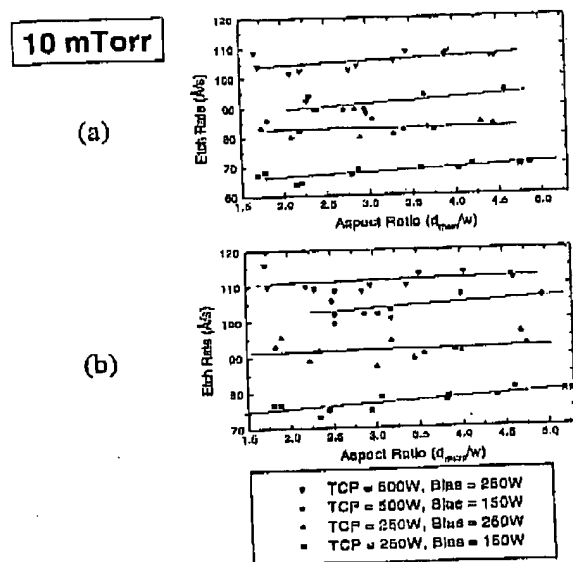


Fig. 7. Etch rate vs aspect ratio at 10 mTorr calculated using (a)  $d_{min}$  and (b)  $d_{max}$ .

right. The vertical axis represents bias power. Profiles etched with 150 W bias power applied are shown at the bottom, and those etched with 250 W bias power applied are on top.

Features (nominally 0.6  $\mu\text{m}$ ) etched at 2 and 10 mTorr, are shown in Figs. 9 and 10, respectively. From these figures,

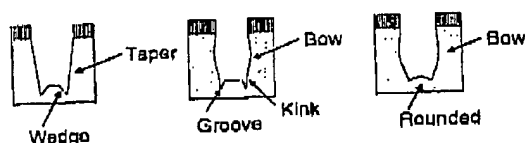


Fig. 8. Illustration of trench profiles and associated terminology used in this work.

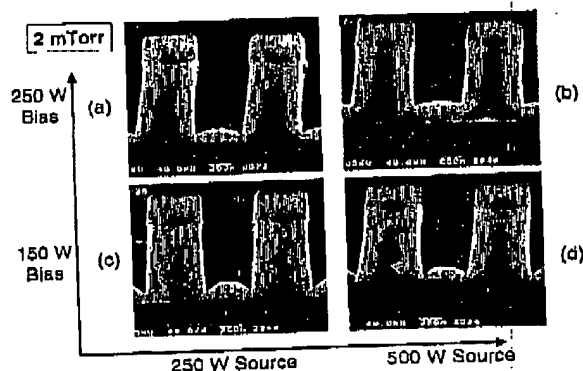


Fig. 9. Cross sections of nominally 0.60  $\mu\text{m}$  nested trenches etched with different source and bias powers at 2 mTorr, 80 sccm  $\text{Cl}_2$ .

JVST A - Vacuum, Surfaces, and Films

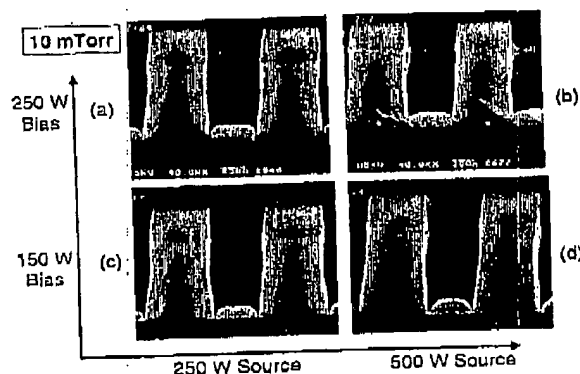


Fig. 10. Cross sections of nominally 0.60  $\mu\text{m}$  nested trenches etched with different source and bias powers at 10 mTorr, 80 sccm  $\text{Cl}_2$ .

it becomes clear that the shape of the feature bottom and sidewall are closely related. Features that develop a sidewall bow with a second point of inflection ("kink") near the bottom of the trench [Figs. 10(a), 10(c), and 10(d)] also develop acute microtrenches ("grooves") in the trench bottoms. Features that develop evenly tapered or bowed sidewalls [Figs. 9(a) and 10(b)] either develop rounded bottoms [Figs. 9(a), 9(b), and 10(b)] or bottoms with broad microtrenches ["wedges," Figs. 9(c) and 9(d)].

This correlation between sidewall contour and microtrench behavior is consistent with the mechanism of ion reflection. The development of bowed sidewalls may cause ions to "focus" at the trench bottom in different ways. A more acute sidewall angle or kink may focus reflecting ions to a smaller area, causing grooves. The development of the sidewalls themselves is less easily explained. The sidewall bow and sidewall kink that we observe have been attributed

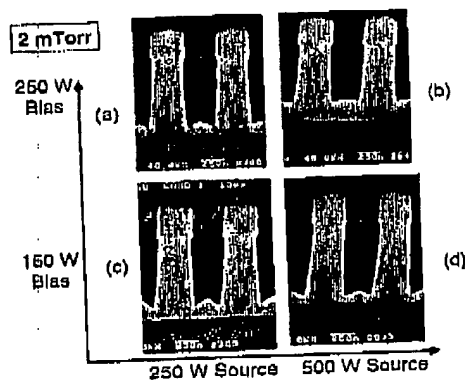


Fig. 11. Cross sections of nominally 0.35  $\mu\text{m}$  nested trenches etched with different source and bias powers at 2 mTorr, 80 sccm  $\text{Cl}_2$ .

BEST AVAILABLE COPY

192

Lane et al.: Feature evolution during plasma etching

192

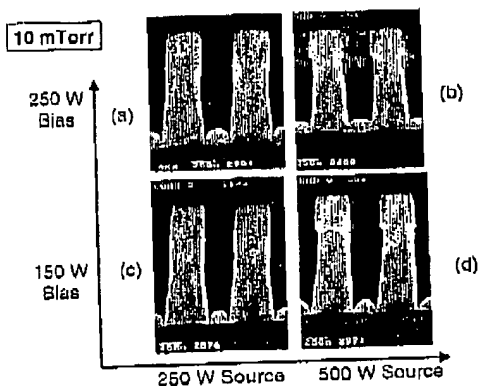


FIG. 12. Cross sections of nominally  $0.35\ \mu\text{m}$  nested trenches etched with different source and bias powers at 10 mTorr, 80 sccm  $\text{Cl}_2$ .

to the different deposition mechanisms that occur during etching combined with off-angle ion bombardment of the sidewall.<sup>13,22</sup> Sidewall kinks and grooves are observed at 10 and not at 2 mTorr. This could be attributed to increased deposition within the trench at 10 mTorr and/or a change in ion angular distribution at the wafer at lower pressures.

A similar analysis holds for Figs. 11 and 12, where nominally  $0.35\ \mu\text{m}$  features are shown at 2 and 10 mTorr, respectively. Wedges overlap in  $0.35\ \mu\text{m}$  features, forming pyramidal trench bottoms [Figs. 11(a), 11(c), and 11(d)]. Again, it is observed that features with kinked sidewalls [Figs. 12(a), 12(c), and 12(d)] also exhibit grooves at the trench bottoms. At narrower feature widths, we also observe more severe undercutting of the oxide hardmask [Figs. 11, 12(b), and 12(d)]. This undercutting has been attributed to ion scattering off the neighboring hardmask.<sup>6,23</sup> Ions scattering off the hardmask at a constant angle would impact the sidewall of a neighboring feature. As the feature width shrinks, the ions impact higher on the neighboring sidewall, causing the observed undercut. This is further corroborated by the fact that no undercutting is observed in open areas, as discussed in Sec. III D. A more detailed discussion of the relationship between profile development and the variables of pressure, source power, and bias power is undertaken below.

### 1. Pressure

Chlorine etching at 2, 10, 25, and 50 mTorr was examined in this study. Cross sections of nominally  $0.35\ \mu\text{m}$  nested trenches etched at 2, 10, 25, and 50 mTorr with a constant 250 W source power, 150 W bias power, and 80 sccm  $\text{Cl}_2$  are shown in Fig. 13. The difference in trench profiles as chamber pressure was varied is striking. At 2 mTorr wedges overlap, forming pyramids at the trench bottoms. At 10 mTorr, grooves are observed at trench bottoms in conjunction with kinked sidewalls. At 25 mTorr trench bottoms are rounded. At 50 mTorr trench sidewalls flare outward, bringing the trench bottom to a point. The average etching rate and microtrench severity with increasing pressure is shown in Fig. 14. The severity of the microtrench was quantified, as

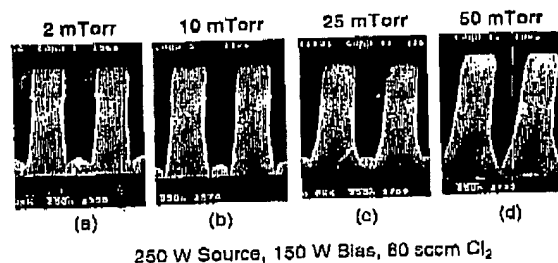


FIG. 13. Cross sections of nominally  $0.35\ \mu\text{m}$  nested trenches etched with 250 W source power, 150 W bias power, 80 sccm  $\text{Cl}_2$ , and (a) 2, (b) 10, (c) 25, and (d) 50 mTorr chamber pressure.

defined in Sec. II B, such that "percent microtrenching"  $= [(d_{\text{micro}} - d_{\text{main}})/d_{\text{main}}] \times 100$ . The etching rate is highest at 10 mTorr, and slowest at 2 and 50 mTorr. Microtrench severity is roughly the same at 2 and 10 mTorr. At 50 mTorr, however, this metric becomes a misnomer as the sidewall taper dominates the profile evolution and causes the trench bottom to come to a point. Undercut of the oxide hardmask is observed at 2 mTorr, decreases at 10 mTorr, and is not observed at 25 or 50 mTorr, suggesting that this phenomenon is insensitive to the broad ion angular distribution at higher pressures. As pressure is increased to 50 mTorr, ions are more likely to endure a collision within the sheath or presheath region, widening the angular distribution. If a wider distribution caused more ions to be reflected at greater angles from the neighboring hardmask, greater undercut would be expected at higher pressures. This is not borne out in the data. The  $\text{SiO}_2$  mask is faceted at 25 mTorr, with the size of the facet increasing at 50 mTorr. The change in angle of the mask sidewall may alter scattered ion trajectories enough to eliminate the mask undercut.

### 2. Source power

The results of etching features (nominally  $0.60\ \mu\text{m}$ ) at 250, 500, and 750 W source powers with a constant 150 W bias power, 10 mTorr, and 80 sccm  $\text{Cl}_2$  are shown in Fig. 15. Again, the correlation between microtrench formation and sidewall shape is noted. At 250 W source power, the side-

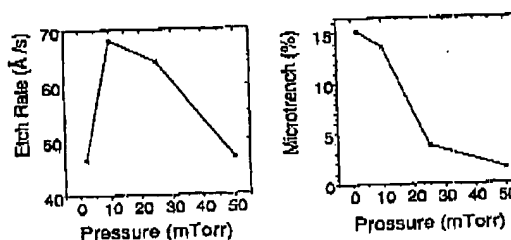


FIG. 14. Average etching rate and microtrench severity for varying chamber pressures and 250 W source power, 150 W bias power, 80 sccm  $\text{Cl}_2$ .

## BEST AVAILABLE COPY

193

Lane et al.: Feature evolution during plasma etching

193

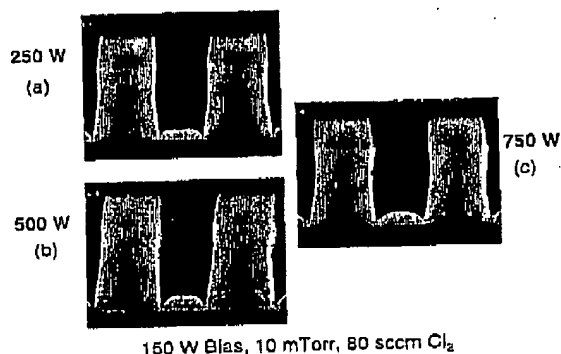


FIG. 15. Cross sections of nominally  $0.60\ \mu\text{m}$  nested trenches etched with 150 W bias power, 10 mTorr chamber pressure, 80 sccm  $\text{Cl}_2$ , and (a) 250 W source power, (b) 500 W source power, and (c) 750 W source power.

wall kink may focus ions to form a groove. The more gradual sidewall bow at 500 and 750 W may defocus scattered ions to form a broader wedge.

Plots of average etching rate and microtrench severity with increasing source power and constant 150 W bias power, 10 mTorr, and 80 sccm  $\text{Cl}_2$  are shown in Fig. 16. As expected, increasing source power—and therefore increasing ion flux—increases etching rates, even as the bias voltage decreases.<sup>24</sup> The sharp decrease in microtrench severity observed at 750 W source power is due to broadening and overlapping of microtrenches. The actual bias voltage could not be directly measured on the etch tool used in this study.

Smaller features (nominally  $0.35\ \mu\text{m}$ ) were etched with 250, 500, and 750 W source powers with a constant 150 W bias power, 10 mTorr, and 80 sccm  $\text{Cl}_2$ , and are shown in Fig. 17. Here, the effect of source power on hardmask undercut is more clearly observed. While there is very little undercut of the oxide mask at 250 W source power, the undercut becomes pronounced at 500 and 750 W source power. This suggests that the undercut phenomenon is more sensitive to the flux of ions impinging on the neighboring hardmask than the ion energy.

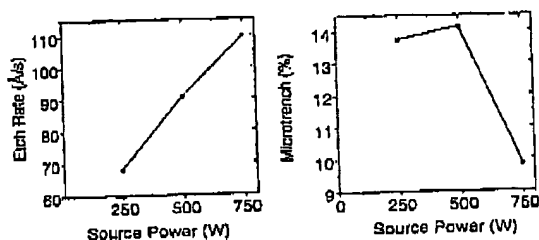


FIG. 16. Average etching rate and microtrench severity for varying source powers and 150 W bias power, 10 mTorr chamber pressure, and 80 sccm  $\text{Cl}_2$ .

JVST A - Vacuum, Surfaces, and Films

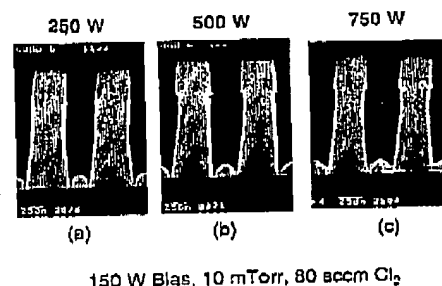


FIG. 17. Cross sections of nominally  $0.35\ \mu\text{m}$  nested trenches etched with 150 W bias power, 10 mTorr chamber pressure, 80 sccm  $\text{Cl}_2$ , and (a) 250 W source power, (b) 500 W source power, and (c) 750 W source power.

### 3. Bias power

Chlorine etching with 150, 250, and 350 W applied bias power was examined in this study. Figure 18 shows cross sections of nominally  $0.35\ \mu\text{m}$  nested trenches etched with 150, 250, and 350 W bias power and a constant 500 W source power, 10 mTorr, and 80 sccm  $\text{Cl}_2$ . As was shown in Figs. 9–12, increasing bias power broadens microtrenches and flattens trench bottoms. The reduction in microtrench severity is even more evident at 350 W bias power [Fig. 18(c)] and leads to complete elimination of microtrenches. In contrast to the variation of other plasma parameters, the change in microtrench profile with increasing bias power appears to be independent of sidewall shape. This is shown in Fig. 18(c), where a markedly bowed sidewall is accompanied by a flat trench bottom. This suggests that the effect of increasing bias power, and therefore increasing ion energy, dominates the ion focusing mechanism. The angular distribution of ions at the wafer surface becomes narrower as the bias power, and ion energy, is increased.<sup>25</sup> Higher energy ions are less affected by collisions in the sheath or presheath region. In a narrow ion distribution, fewer ions impinge on and are focused by the sidewall, resulting in a flatter trench bottom. A summary of this effect is shown in Fig. 19 with

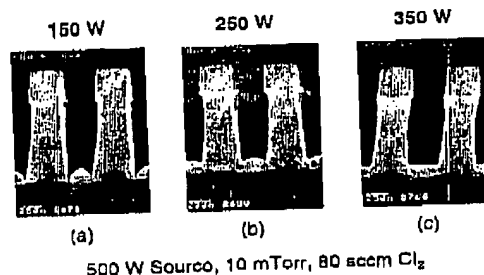


FIG. 18. Cross sections of nominally  $0.35\ \mu\text{m}$  nested trenches etched with 500 W source power, 10 mTorr chamber pressure, 80 sccm  $\text{Cl}_2$ , and (a) 150 W bias power, (b) 250 W bias power, and (c) 350 W bias power.

## BEST AVAILABLE COPY

194

Lane et al.: Feature evolution during plasma etching

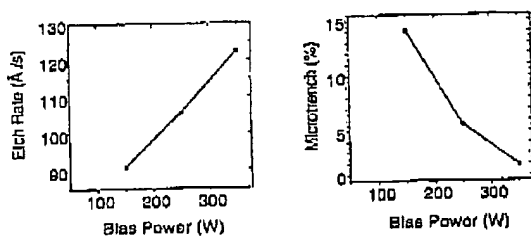


FIG. 19. Average etching rate and microtrench severity for varying bias powers and 500 W source power, 10 mTorr chamber pressure, and 80 sccm  $\text{Cl}_2$ .

plots of etching rates and microtrench severity as a function of bias power. Etching rates increase while microtrench severity decreases with increased bias power.

### C. Isolated trenches

Isolated trenches exhibited similar behavior to their nested trench counterparts, except for slight variations in the microfeature profile. Isolated trench bottoms always exhibited slightly wider, less severe microfeatures than nested trenches. Two cases (Table 1, conditions 1 and 3) of nominally  $0.35 \mu\text{m}$  isolated trenches are shown in Fig. 20. Comparing Figs. 11(a) and 20(a) reveal a slight rounding of the isolated trench bottom compared to the nested trench in Fig. 11. Isolated trenches also tended to exhibit smaller grooves at high source power and pressure than observed in nested trenches. This can be seen by comparing Fig. 12(c) to Fig. 20(b), and can be attributed variations in lithography where isolated trenches were slightly wider than the nested features nominally the same width.

### D. Isolated lines

Isolated lines had the same microfeature profile at the base of the line as with the largest (nominally  $0.60 \mu\text{m}$ )

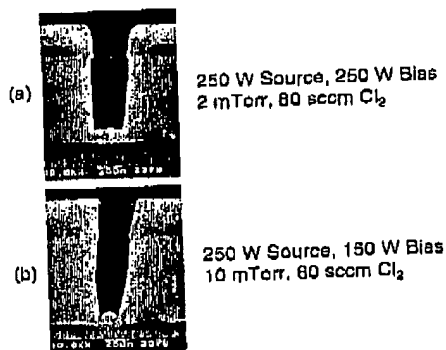
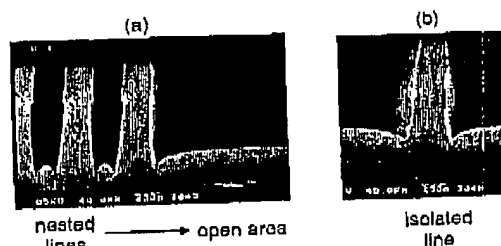


FIG. 20. Cross sections of nominally  $0.35 \mu\text{m}$  isolated trenches etched with (a) 250 W source power, 250 W bias power, 2 mTorr chamber pressure, and 80 sccm  $\text{Cl}_2$ ; (b) 250 W source power, 150 W bias power, 10 mTorr, and 80 sccm  $\text{Cl}_2$ .



40 sccm  $\text{Cl}_2$ , 500 W source, 150 W bias, 10 mTorr

FIG. 21. Cross sections of (a) edge of a series of nested lines (nominally  $0.35 \mu\text{m}$ ) and open area and (b) isolated line (nominally  $0.35 \mu\text{m}$ ) etched with 40 sccm  $\text{Cl}_2$ , 500 W source power, 150 W bias power, and 10 mTorr chamber pressure.

nested features. The striking difference between isolated line profiles and nested line profiles was the lack of mask undercut in isolated lines under any plasma condition. The end of a group of nested lines as well as an isolated line etched with 40 sccm  $\text{Cl}_2$ , 10 mTorr, 500 W source power, and 250 W bias power is shown in Fig. 21. On the open area side of the last nested line, the oxide hardmask is not undercut. In contrast, the last nested line does undercut the oxide mask on the nested area side. This is consistent with the mechanism of ion reflection from the neighboring hardmask. In isolated lines, where there is no neighbor, no undercut is observed. The sidewall on the open area of this last nested line is identical to the sidewall of the isolated line, and not the nested lines. Specifically, the nested line sidewalls are tapered while the isolated line sidewalls are vertical with a slight flare at the bottom. This sidewall discrepancy is shared across all conditions and may simply be caused by the presence of a nearest neighbor line.

Two isolated lines [Figs. 22(a) and 22(b) correspond to Table 1, conditions 5 and 4, respectively] are shown in Fig.

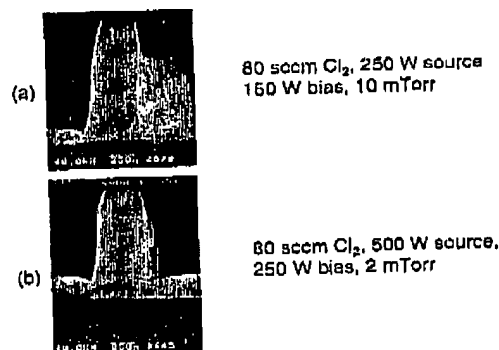


FIG. 22. Cross sections of nominally  $0.6 \mu\text{m}$  isolated lines etched with (a) 80 sccm  $\text{Cl}_2$ , 250 W source power, 150 W bias power, and 10 mTorr chamber pressure; (b) 80 sccm  $\text{Cl}_2$ , 500 W source power, 250 W bias power, and 2 mTorr chamber pressure.

## BEST AVAILABLE COPY

195

Lane et al.: Feature evolution during plasma etching

195

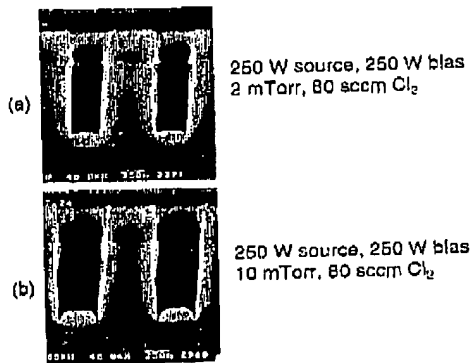


FIG. 23. Cross sections of windows nominally  $0.35 \mu\text{m}$  etched with (a) 250 W source power, 250 W bias power, 2 mTorr chamber pressure, and 80 sccm  $\text{Cl}_2$ ; (b) 250 W source power, 250 W bias power, 10 mTorr, and 80 sccm  $\text{Cl}_2$ .

22. Comparing Fig. 22(a) with the corresponding features in Figs. 10(c) and 12(c), it is evident that the sidewall kink and groove are maintained in the isolated line. The groove, however, is more severe within the nested features. Comparing Fig. 22(b) with the corresponding features in Figs. 9(b) and 11(b), it is observed that the sidewall bow and feature bottom rounding is preserved in the open area and feature bottom undercut is eliminated.

### E. Windows

Etched windows, or vias, possessed the same sidewall profiles as their nested trench counterparts. The window bottom profile, however, tended to resemble the isolated trench profile in that the severity of microtrenches was reduced compared to the nested trenches. Two examples of windows [Fig. 23(a) and 23(b) correspond to Table I, conditions 3 and 7, respectively] are shown in Fig. 23. In comparing Fig. 23(a) with the corresponding nested trench [Fig. 11(a)] and isolated trench [Fig. 20(a)], it is evident that the window feature bottom is more rounded than its trench counterparts. In conditions where grooves were observed in the nested trenches, windows exhibited similar profile development [compare Fig. 23(b) with Figs. 10(a) and 12(a)].

Windows often had smoother, flatter bottoms than even the isolated trenches. This is consistent with the fact that a window is a more "closed" feature. For windows, the three-dimensional effects of ion reflection must be considered. Under plasma conditions that result in broad microtrenches, the three-dimensional ion focusing in windows could flatten the window bottoms further, as the broad microtrenches can overlap in three dimensions. Under plasma conditions that result in narrow grooves, however, no overlapping occurs, and the three-dimensional effects fail to play a significant role.

JVST A - Vacuum, Surfaces, and Films

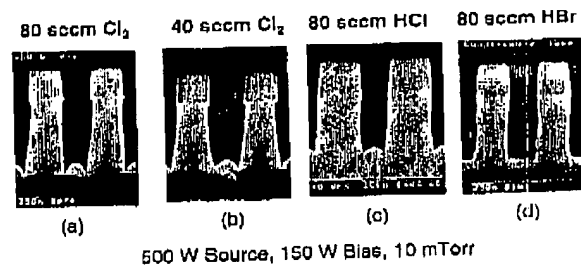


FIG. 24. Cross sections of nominally  $0.35 \mu\text{m}$  nested trenches etched with 500 W source power, 150 W bias power, 10 mTorr chamber pressure and (a) 80 sccm  $\text{Cl}_2$ , (b) 40 sccm  $\text{Cl}_2$ , (c) 80 sccm  $\text{HCl}$  ( $0.6 \mu\text{m}$ ), and (d) 80 sccm  $\text{HBr}$ .

### F. Feed gas composition and flow rate

Etching of silicon often uses halogenated gases in addition to  $\text{Cl}_2$ . In this study, the effects of  $\text{Cl}_2$ ,  $\text{HCl}$ , and  $\text{HBr}$  on feature profile evolution were investigated. Wafers were etched at 500 W source power, 150 W bias power, and 10 mTorr pressure with  $\text{Cl}_2$ ,  $\text{HBr}$ , and  $\text{HCl}$  plasmas. Cross sections of nominally  $0.35 \mu\text{m}$  nested trenches ( $0.4 \mu\text{m}$  for  $\text{HCl}$ ) etched under these conditions are shown in Fig. 24. Trenches etched with  $\text{HBr}$  have much flatter trench bottoms. Trenches etched by plasmas containing chlorine ( $\text{Cl}_2$  or  $\text{HCl}$ ) have tapered/bowed sidewalls with an undercut oxide hard-mask and sharp microtrenches. An additional experiment was conducted to investigate the effect of increasing residence time in the reactor and the  $\text{Cl}_2$  flow was reduced from 80 to 40 sccm. The resulting profile is shown in Fig. 24(b) and any difference between Figs. 24(b) and 24(a) (80 sccm) is slight.

Average etching rates and microtrench severity for different feed gases are shown in Fig. 25. Etching rates were fastest in  $\text{Cl}_2$ , slower in  $\text{HCl}$ , and slowest in a  $\text{HBr}$  plasma. Microtrench severity was dramatically reduced in  $\text{HBr}$  plasmas. The reduction in the etching rate with decreasing halogen reactivity has been reported previously, and may account for the decrease in microtrench severity. Other investigations from this laboratory have shown that ideal trench profiles (straight sidewalls/flat bottoms) form in  $\text{HBr}$  plasma etching of Si if oxygen is present in either the feed gas or from the presence of a  $\text{SiO}_2$  mask.<sup>26</sup>

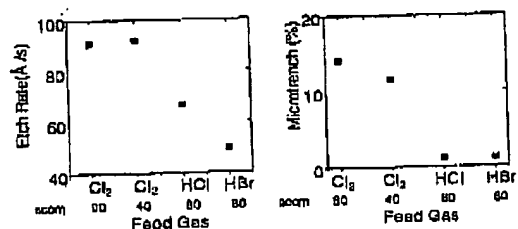


FIG. 25. Average etching rate and microtrench severity for varying feed gases, flow, and constant 500 W source power, 150 W bias power, and 10 mTorr chamber pressure.

## BEST AVAILABLE COPY

196

Lane et al.: Feature evolution during plasma etching

196

## IV. SUMMARY

A fundamental study into feature evolution during the high-density plasma etching of poly-Si was conducted, duplicating and expanding a sister study of Si(100) etching. Results are consistent between the two studies, suggesting that the crystalline structure plays a limited role in profile development during  $\text{Cl}_2$  plasma etching.

Etching rates were found to increase as source power increased from 250 to 750 W, and as bias power increased from 150 to 350 W. Etching rates increased as pressure increased from 2 to 10 mTorr and decreased as pressure was further increased to 25 and 50 mTorr. Etching rates were highest in a  $\text{Cl}_2$  plasma, lower in a HCl plasma, and lowest in a HBr plasma.

Microtrenching was found to be a strong function of plasma parameters. Increasing source power from 250 to 750 W broadened microtrenches. Increasing bias power from 150 to 350 W eliminated microtrenching. Increasing pressure qualitatively changed the shape of microtrenches from a wedge shape at 2 mTorr, to a groove at 10 mTorr. An acute sidewall flare at 25 and 50 mTorr dominated the trench profile, minimizing microtrench formation. Microtrenches were only observed in a  $\text{Cl}_2$  or HCl plasmas, not during etching with HBr.

Nested trenches, nested lines, isolated lines, isolated trenches, and windows all exhibited the same qualitative profile development and trends across plasma conditions. Isolated trenches, however, exhibited less severe microtrenches. In plasma conditions where nested features developed rounded bottoms or wedges, windows exhibited even milder broad or rounded trench bottoms. In conditions where nested features developed grooves, windows exhibited similar profile development. Isolated lines exhibited qualitatively similar profile development to nested features. However, the undercut of the hardmask was never observed in isolated lines.

These observations are consistent with the mechanism of microtrench formation by focusing ions off a tapered or bowed sidewall. Grooves were always observed in conjunction with a sidewall kink near the bottom of the trench. Rounded trench bottoms or wedges were observed in conjunction with evenly tapered or bowed sidewalls. The exception to this is at high bias power, where flat trench bottoms appeared in conjunction with bowed sidewalls.

## ACKNOWLEDGMENTS

The authors would like to thank V. M. Donnelly, A. Kornblit, and H. L. Maynard for enlightening discussions. The authors thank M. Cerullo, C.-P. Chang, H. Lee, and J. Miner for assistance with the SEM and the Silicon Fabrication Research Laboratory staff for assistance with wafer fabrication.

- <sup>1</sup>H. Hübner and M. Engelhardt, *J. Electrochem. Soc.* **141**, 2453 (1994).
- <sup>2</sup>J. I. Ulman, C. J. Peri, and J. P. McVittie, *J. Electrochem. Soc.* **135**, 1521 (1988).
- <sup>3</sup>E. S. G. Shaqfeh and C. W. Jurgensen, *J. Appl. Phys.* **66**, 4664 (1989).
- <sup>4</sup>A. C. Westerhelm, A. H. Labun, J. H. Dabash, J. C. Arnold, H. H. Sawin, and V. Yu-Wing, *J. Vac. Sci. Technol. A* **13**, 853 (1995).
- <sup>5</sup>R. A. Gottschin and C. W. Jurgensen, *J. Vac. Sci. Technol. B* **10**, 2133 (1992).
- <sup>6</sup>G. S. Hwang, C. M. Anderson, M. J. Gordon, T. A. Moore, T. K. Minton, and K. P. Gilpin, *Phys. Rev. Lett.* **77**, 3049 (1996).
- <sup>7</sup>S. V. Nguyen, D. Dubuzinsky, S. R. Stiffler, and G. Christman, *J. Electrochem. Soc.* **138**, 1112 (1991).
- <sup>8</sup>R. J. Haekstra, M. J. Kasher, V. Sukharev, and P. Schoenborn, *J. Vac. Sci. Technol. B* **16**, 2102 (1998).
- <sup>9</sup>J. C. Arnold and H. H. Sawin, *J. Appl. Phys.* **70**, 5314 (1991).
- <sup>10</sup>S. Miyakawa and J. P. McVittie, *Jpn. J. Appl. Phys., Part 1* **33**, 2184 (1994).
- <sup>11</sup>M. Schaepekens and G. S. Oehrlein, *Appl. Phys. Lett.* **72**, 1293 (1998).
- <sup>12</sup>G. S. Hwang and K. P. Gilpin, *J. Appl. Phys.* **81**, 3433 (1997).
- <sup>13</sup>Y.-J. Lii and J. Jorne, *J. Electrochem. Soc.* **137**, 2837 (1990).
- <sup>14</sup>C. Lee, D. B. Graves, and M. A. Lieberman, *Plasma Chem. Plasma Process.* **16**, 99 (1996).
- <sup>15</sup>M. Tada, K. Ono, and K. Nishikawa, *J. Vac. Sci. Technol. B* **14**, 3291 (1996).
- <sup>16</sup>J. P. Chang, A. P. Mahonvala, and H. H. Sawin, *J. Vac. Sci. Technol. A* **16**, 217 (1998).
- <sup>17</sup>J. I. Ulman and J. P. McVittie, *J. Appl. Phys.* **65**, 1484 (1989).
- <sup>18</sup>J. A. Levinson, E. S. G. Shaqfeh, M. Balouch, and A. V. Hamza, *J. Vac. Sci. Technol. A* **15**, 1902 (1997).
- <sup>19</sup>T. J. Dalton, J. C. Arnold, H. H. Sawin, S. Swain, and D. Carliss, *J. Electrochem. Soc.* **140**, 2395 (1993).
- <sup>20</sup>M. A. Vyvoda et al., *J. Vac. Sci. Technol. A* **16**, 1 (1998).
- <sup>21</sup>LAM Research Corp., Fremont, CA; URL <http://www.lamre.com>
- <sup>22</sup>M. Tada and K. Ono, *Jpn. J. Appl. Phys., Part 1* **36**, 2482 (1997).
- <sup>23</sup>S. Ohki, M. Oda, H. Akiya, and T. Shibata, *J. Vac. Sci. Technol. B* **5**, 1611 (1987).
- <sup>24</sup>K. H. A. Bogart, F. P. Klemens, M. V. Malyshev, J. I. Connell, V. M. Donnelly, and J. T. C. Lee, *J. Vac. Sci. Technol. A* **18**, 197 (2000).
- <sup>25</sup>J. Zheng, K. P. Brinkmann, and J. P. McVittie, *J. Vac. Sci. Technol. A* **13**, 849 (1995).
- <sup>26</sup>J. M. Lane, F. P. Klemens, K. H. A. Bogart, and J. T. C. Lee, *J. Vac. Sci. Technol. A*, (accepted).